PURDUE UNIVERSITY
GRADUATE SCHOOL
Thesis/Dissertation Acceptance

This is to certify that the thesis/dissertation prepared

By Yi Cui

Entitled

Studies of Rechargeable Lithium-Sulfur Batteries

For the degree of Master of Science in Mechanical Engineering

Is approved by the final examining committee:

Yongzhu Fu
Chair

Jian Xie

Likun Zhu

To the best of my knowledge and as understood by the student in the Thesis/Dissertation Agreement, Publication Delay, and Certification Disclaimer (Graduate School Form 32), this thesis/dissertation adheres to the provisions of Purdue University's "Policy of Integrity in Research" and the use of copyright material.

Approved by Major Professor(s): Yongzhu Fu

Approved by: Sohel Anwar 4/21/2016

Head of the Departmental Graduate Program Date

STUDIES OF RECHARGEABLE LITHIUM-SULFUR BATTERIES

A Thesis

Submitted to the Faculty

of

Purdue University

by

Yi Cui

In Partial Fulfillment of the

Requirements for the Degree

of

Master of Science in Mechanical Engineering

May 2016

Purdue University

Indianapolis, Indiana

This thesis is dedicated to my dear parents for their unconditional love and strong support for my study and research which lead me the path to success. I would also like to thank my girlfriend for giving me a happy and relaxed time which maintains my research motivation. They gave me strength and confidence when I was down and helped me to step out of the toughness time. Without them, it is impossible for me to finish my master's degree at IUPUI.

ACKNOWLEDGMENTS

First of all, I would like to thank my advisor Dr. Yongzhu Fu who helps me on my research career and the experiment designs for this thesis. He is a brilliant professor who provides me varieties of good ideas that help me to open my minds and expand my views. He also helps me to get used to the lives as a graduate student and supports me to continue my study in financial aspect.

I would also like to thank Amruth Bhargav and Min Wu to discuss with me to give me some ideas. They also help me a lot on my experiments as colleagues. My graduate life will never be so easy without them.

TABLE OF CONTENTS

LIST OF TABLES

LIST OF FIGURES

Figure Page

ABSTRACT

Cui, Yi. M.S.M.E., Purdue University, May 2016. Studies of Rechargeable Lithium-Sulfur Batteries. Major Professor: Yongzhu Fu.

The studies of rechargeable lithium-sulfur (Li-S) batteries are included in this thesis.

In the first part of this thesis, a linear sweep voltammetry method to study polysulfide transport through separators is presented. Shuttle of polysulfide from the sulfur cathode to lithium metal anode in rechargeable Li-S batteries is a critical issue hindering cycling efficiency and life. Several approaches have been developed to minimize it including polysulfide-blocking separators; there is a need for measuring polysulfide transport through separators. We have developed a linear sweep voltammetry method to measure the anodic (oxidization) current of polysulfides crossed separators, which can be used as a quantitative measurement of the polysulfide transport through separators. The electrochemical oxidation of polysulfide is diffusion controlled. The electrical charge in Coulombs produced by the oxidation of polysulfide is linearly related to the concentration of polysulfide within a certain range (≤ 0.5 M). Separators with a high porosity (large pore size) show high anodic currents, resulting in fast capacity degradation and low Coulombic efficiencies in Li-S cells. These results demonstrate this method can be used to correlate the polysulfide transport through separators with the separator structure and battery performance, therefore provide guidance for developing new separators for Li-S batteries.

The second part includes a study on improving cycling performance of Li/polysulfide batteries by applying a functional polymer on carbon current collector. Significant capacity decay over cycling in Li-S batteries is a major impediment for their practical applications. Polysulfides Li_2S_x ($3 < x \leq 8$) formed in the cycling are soluble

in liquid electrolyte, which is the main reason for capacity loss and cycling instability. Functional polymers can tune the structure and property of sulfur electrodes, hold polysulfides, and improve cycle life. We have examined a polyvinylpyrrolidone-modified carbon paper (CP-PVP) current collector in Li/polysulfide cells. PVP is soluble in the electrolyte solvent, but shows strong affinity with lithium polysulfides. The retention of polysulfides in the CP-PVP current collector is improved by $\sim 50\%$, which is measured by a linear sweep voltammetry method. Without $LiNO_3$ additive in the electrolyte, the CP-PVP current collector with 50 ug of PVP can significantly improve cycling stability with a capacity retention of $> 90\%$ over 50 cycles at C/10 rate. With $LiNO_3$ additive in the electrolyte, the cell shows a reversible capacity of > 1000 mAh g^{-1} and a capacity retention of $> 80\%$ over 100 cycles at C/5 rate.

The third part of this thesis is about a study on a binder-free sulfur/carbon composite electrode prepared by a sulfur sublimation method for Li-S batteries. Sulfur nanoparticles fill large pores in a carbon paper substrate and primarily has a monoclinic crystal structure. The composite electrode shows a long cycle life of over 200 cycles with a good rate performance in Li-S batteries.

1. INTRODUCTION

With the increasing demand of advanced devices and high quality lives in modern society, the requirement of energy is getting ever growing. After the industrial revolution, the conventional non-renewable fossil fuels, such as gasoline, natural gas and coal, were widely used in people's lives and industrial manufacture. However, these conventional energies caused more and more serious pollution problems on the earth environment, like global warming, ocean pollution and atmosphere damage. Those phenomena led people to solve the problems by studying and applying other sources of renewable energy instead of traditional fossil fuels. Rechargeable batteries, solar energy, wind energy and fuel cells are resolved solutions that have been widely known by people and applied in our daily lives for replacing conventional energy [1–6]. Compared with the intermittent wind and solar energy, rechargeable batteries can be used as more competitive energy sources and more effective electrical energy storages, which make rechargeable batteries as one important option among these renewable energies.

In the rechargeable battery system, a variety of kinds of batteries, such as lead-acid, nickel metal hybrid, nickel-cadmium, lithium ion batteries et al., have been applied and served our society for over a century [7–12]. For instance, lead-acid batteries are used as storage batteries in automobiles, and lithium ion batteries are widely applied in cell phones, laptops and the other portable electronic devices. Especially, lithium ion batteries have become prominent electrical storage for portable devices in the last two decades. Recently, lithium ion batteries are successfully applied in Tesla vehicles to replace the conventional internal combustion engines, which offer high energy density and power for the vehicles. In addition, Toyota applied batteries in hybrid vehicles for saving gasoline, which make the cars more environmental friendly and economic. So far, more and more companies start to develop new automobiles

with rechargeable batteries. This approach demonstrates a high application potential of rechargeable batteries in the future, including Li-S batteries, Li-air batteries and flow batteries [13–16].

Among rechargeable batteries, lithium-sulfur (Li-S) batteries are one novel battery system which attract more and more attention and expectation. The concept of applying sulfur as a positive electrode material in storage batteries was proposed by Herbet and Ulam in 1962. The first generation of electrolytes was identified to be alkaline perchlorate, bromide or chlorate dissolved in amine based solvents. Later in 1966, high-energy-density metal-sulfur batteries with organic electrolyte was proposed and the theoretical energy densities of metal-sulfur batteries was calculated and presented. The electrolytes consists of one or two of solvents, which are propylene carbonate, dimethylformamide, dimethyl sulfoxide or γ-butyrolactone. Later on an important development of Li-S batteries, the electrolytes were changed to propylene carbonate system, tetrahydrofuran (THF)-toluene and then the mixtures of dioxolane-based electrolyte, which are being widely used now.

Starting from 2000, many efforts have been focused on rechargeable Li-S batteries with rising number of publications. Li-S batteries have become an important focus of energy storage research over the past decades because of the high specific capacity of the sulfur cathode (i.e., 1672 mAh g^{-1}) and high theoretical specific energy (i.e., 2600 Wh kg^{-1}) [17–19]. Lithium ion batteries have high specific energy because of the high cell voltage due to the metal oxide cathodes used, as shown in Fig. 1.1. Comparing to Li-ion batteries, which have limited capacities of 100-250 mAh g^{-1} in transition metal oxide cathodes [20,21], Li-S batteries can potentially provide 2-3 times of higher specific energies. In addition, sulfur has several appealing characteristics such as low cost, abundance, and environmental benignity. Therefore, Li-S batteries are considered as a promising next-generation rechargeable battery.

However, the commercial applications of Li-S batteries are not quite successful despite that many significant improvements have been made in the past decades. During an ideal discharge process, S_8 is reduced to form high-order lithium polysulfides Li_2S_x

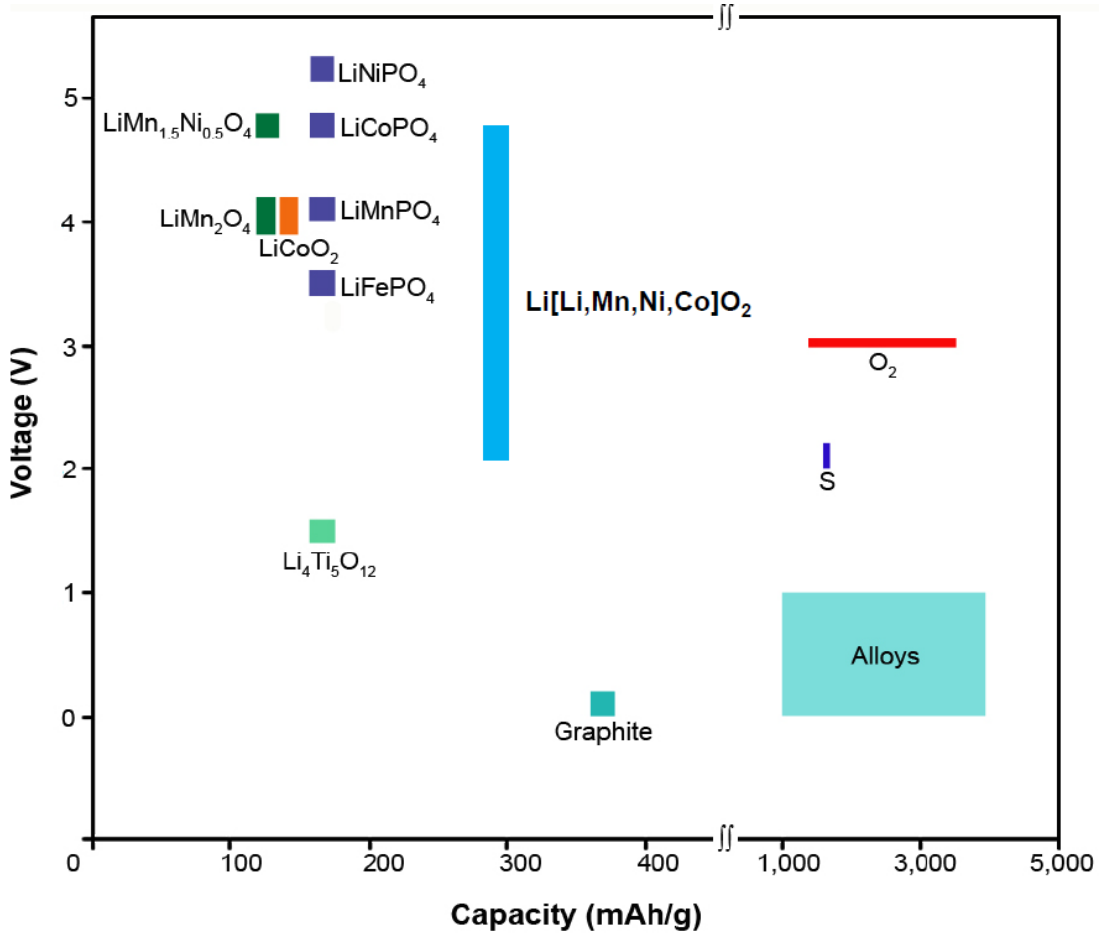

Figure 1.1. Voltage and capacity ranges of some cathode and anode materials. Reprinted with permission from ref 17. Copyright 2011 American Chemical Society.

($6 < x \leq 8$). In the continuous discharge process, lower order lithium polysulfides Li_2S_x ($2 < x \leq 4$) are formed with additional lithium. 2.3 V and 2.1 V are shown as two discharge plateaus with ether-based liquid electrolytes, which represent the reactions of S8 to Li_2S_4 and Li_2S_4 to Li_2S, respectively. In the end, Li_2S is formed as the discharge product, as shown in Fig. 1.2. During charge process, Li_2S is converted to solid sulfur through intermediate products of lithium polysulfides as a reversible process [22]. Sulfur is a natural insulating material (i.e., $5 * 10^{-30}$ S cm^{-1} at 25°C) which leads high resistance in Li-S batteries. The intermediate products of lithium polysulfides (i.e., Li_2S_x, x = 3-8) are soluble in liquid electrolyte, which have transfor-

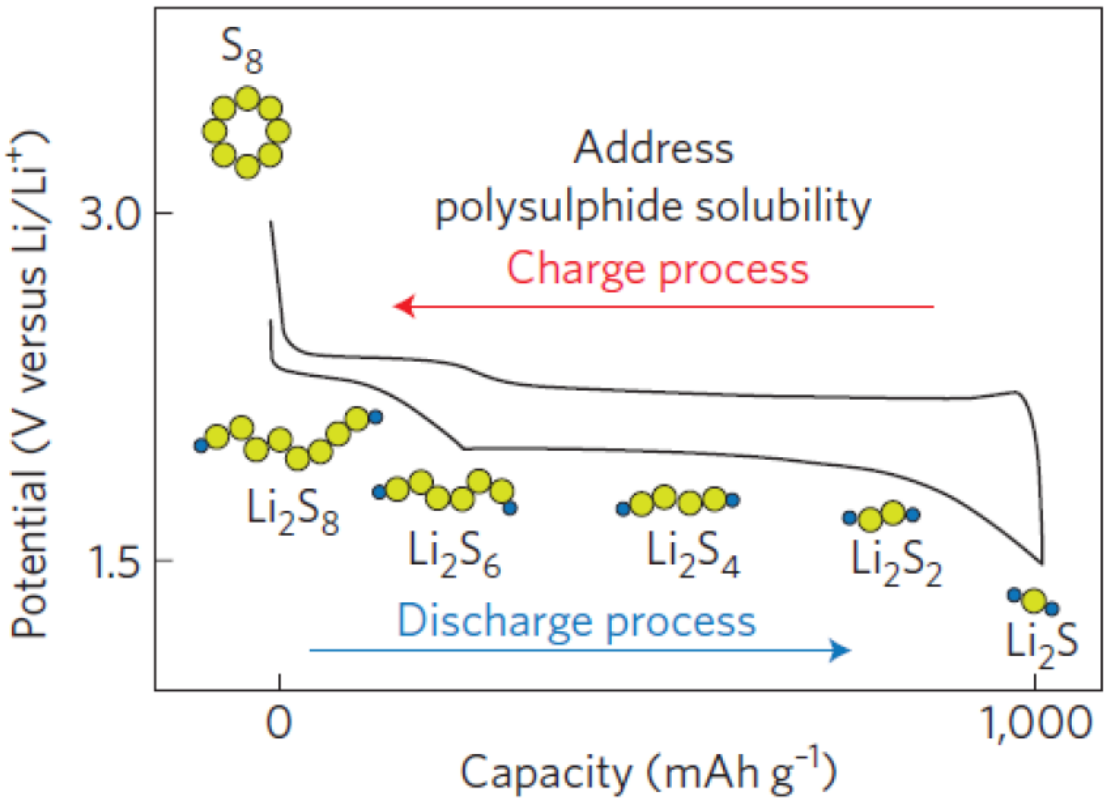

Figure 1.2. Voltage profiles of a Li-S cell. Reprinted with permission from ref 22. Copyright 2011 Nature Publishing Group.

mations of structure and morphology leading unstable electrochemical contact with carbon. In addition, the dissolved polysulfide shuttle through porous separators can react with lithium anode, which results the waste of energy, low Coulombic efficiency and fast capacity fade [23–25]. To overcome these issues, many efforts have been put into studies on Li-S batteries [18, 26, 27].

2. POLYSULFIDE TRANSPORT THROUGH SEPARATORS MEASURED BY A LINEAR VOLTAGE SWEEP METHOD

2.1 Introduction

Lithium polysulfides Li_2S_x (x = 3-8), can dissolve in ether solvents and shuttle through the porous separator (e.g., Celgard® separators) to the lithium metal anode resulting in low Coulombic efficiency and poor cycle life, which make shuttle phenomenon a serious issue in Li-S batteries. To improve the cycling performance of Li-S batteries, the shuttle effect has to be suppressed in order to retain active material in the sulfur cathode. Several approaches have been developed to overcome this issue, such as using porous carbon materials to hold polysulfides in the cathode [28,29], applying a carbon interlayer between the separator and sulfur cathode to block the polysulfide transport [30], and developing new separators to suppress the shuttle effect [31]. As many studies are focused on new separators such as carbon-coated separators and polymer electrolytes, a quantitative and facile method is needed to evaluate the polysulfide transport through these separators.

In 2000, Ren et al. reported a method to evaluate methanol crossover through proton-conducting membranes in direct methanol fuel cells by measuring methanol crossover current [32]. This method has been used in evaluating methanol crossover through a variety of membranes [33,34]. Similarly, polysulfide transport through separators could be measured by a similar approach. Here, we report a linear voltage sweep (LVS) method to evaluate the polysulfide transport through separators by measuring the polysulfide crossover current, which can be correlated with the structure of separators and battery cycling performance. We select polysulfide Li_2S_6 in this study as it can be fully dissolved in liquid electrolyte and it also can be oxidized to elemental sulfur or higher-order polysulfides [35].

2.2 Experimental

2.2.1 Schematic Diagram of the Experimental Cell, Materials and Instruments

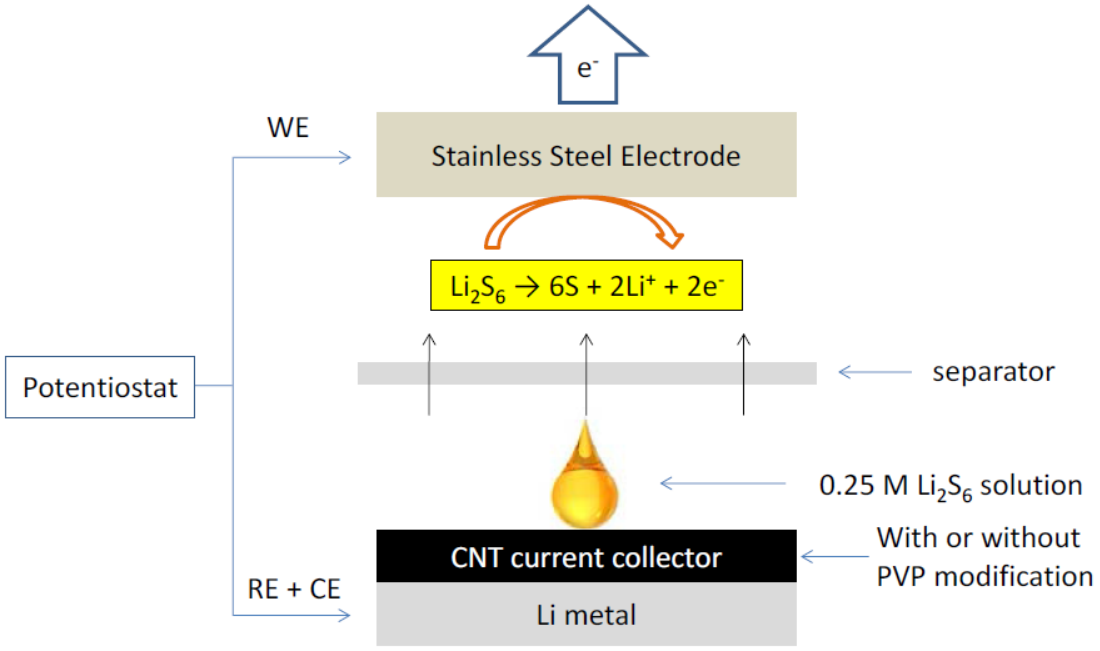

Figure 2.1. Schematic diagram of the experimental cell and working principle. The liquid polysulfide solution was added into the carbon nanotube paper. The arrows show the polysulfide can migrate through the separator to the working electrode and get oxidized to form elemental sulfur. The cell was connected to a potentiostat, WE: working electrode, RE: reference electrode, CE: counter electrode.

All materials used are included in Table 2.1. All instruments used are included in Table 2.2.

2.2.2 Experimental Section

The experimental cell is shown in Fig. 2.1, which was sealed in a home-made Swagelok cell in an Argon-filled glove box (MBraun). The cell consists of a piece of lithium metal (Sigma Aldrich) as the reference and counter electrode, a piece

Table 2.1. Experimental materials

Material name	Purity	Provider
Lithium metal (Li)	99.9%	Sigma Aldrich
Carbon nanotube paper (CNT)	Not specified	NanoTechLabs
Monolayer PP 2400 separator	Not specified	Celgard®
Monolayer PP 2400 separator	Not specified	Celgard®
Trilayer PP/PE/PP 2325 separator	Not specified	Celgard®
Sulfur (S)	99.5%	Alfa Aesar
Sulfur powder (S)	99%	Fisher Scientific
Lithium sulfide (Li_2S)	99.99%, metal trace	Sigma Aldrich
Lithium trifluoromethanesulfonate ($LiCF_3SO_3$)	98%	Acros Organics
Lithium bis(trifluoromethane) sulfonamide (LiTFSI)	98%	Acros Organics
Lithium nitrate ($LiNO_3$)	99+%	Acros Organics
Dimethoxy ethane (DME)	99+%	Acros Organics
1,3-dioxolane (DOL)	99.5%	Acros Organics
Polyvinylpyrrolidone (PVP,Mw = 1, 300, 000)	Not specified	Acros Organics
Anhydrous ethanol	99.5%, 200 proof	Sigma-Aldrich

Table 2.2. Experimental instruments

Instrument name	Provider
Argon-filled glove box	MBraun
Swagelok cell	Home-made
CR2032 coin cells	Not specified
Potentiostat	Bio-Logic VSP
Arbin battery cycler	Not specified
Scanning electron microscope (SEM)	JEOL JSM-7800F
X-ray diffractometer (D8 Discover A25)	Bruker AXS
Gas sorption analyzer (Autosorb iQ)	Quantachrome

(0.97 cm^2) of carbon nanotube (CNT) paper (NanoTechLabs) which was used as a reservoir for holding 50 μL of polysulfide solution added to it, and a stainless steel current collector as the working electrode. A separator was placed in between

the polysulfide-filled CNT paper and stainless steel current collector. The cell was connected to a potentiostat (Bio-Logic VSP) and the LVS was carried out from open circuit voltage of the cell to 4.5 V at various rates. Three Celgard® separators with same thickness (25 μm) were evaluated, which are monolayer PP 2400 (porosity 41%, pore size 43 nm) and 2500 (porosity 55%, pore size 64 nm), and trilayer PP/PE/PP 2325 (porosity 39%, pore size 28 nm).

To prepare the lithium polysulfide (Li_2S_6) solution, stoichiometric amounts of sulfur (Alfa Aesar) and lithium sulfide (Li_2S, Sigma Aldrich) were mixed with 1.0 M lithium trifluoromethanesulfonate ($LiCF_3SO_3$, Acros Organics) in dimethoxy ethane (DME, Acros Organics) and 1,3-dioxolane (DOL, Acros Organics) (1:1, v/v) by stirring overnight. Six polysulfide solutions of different concentration were prepared, which are 0.1 M, 0.175 M, 0.25 M, 0.375 M, 0.5 M and 1.0 M. All the cells were tested within 10 min after the cells were assembled to minimize the amount of polysulfides that reacted with the lithium metal. To evaluate the battery performance of these separators, lithium/dissolved polysulfide cells were selected. Coin cells with the CNT paper as current collector were assembled in the glove box. First, 20 μL of 0.25 M polysulfide solutionwas added into the CNT current collector. Then a Celgard® separator was placed on the top of the CNT paper. 20 μL of blank electrolyte without polysulfide was added on the separator. Finally, the lithium metal anode was placed on the separator. Electrochemical performances of the cells were galvanostatically evaluated with an Arbin battery cycler between 1.5 and 3.0 V at C/5 rate (1C = 1672 mA g^{-1} based on the mass of sulfur in the polysulfide solution). The specific capacity values shown in this paper are calculated by dividing the capacities obtained by the mass of sulfur.

2.3 Results and Discussions

Fig. 2.1 shows the experimental cell setup and the principle of this method. The prepared polysulfide solution contains fully dissolved polysulfide Li_2S_6. In the LVS

measurement, polysulfides can migrate from the CNT paper to the working electrode through the separator as indicated by the arrows in the figure when the potential of the working electrode increases. The intermediate polysulfide Li_2S_6 can be oxidized at the surface of the working electrode to form higherorder polysulfides (e.g., Li_2S_8) or elemental sulfur ($Li_2S_6 \rightarrow 6S + 2Li^+ + 2e^-$). After the measurement, a layer of dark yellow solid material can be seen on the surface of the working electrode, which is the oxidized product of Li_2S_6. Produced lithium ions migrate to the counter electrode and get reduced on the lithium metal surface, whereas the electrons form the anodic (oxidation) current which can be measured by the potentiostat. When 50 μL of 0.25 M Li_2S_6 solution was used in the experiment, the total electrical charge that can be produced is 2.41 Coulombs if all polysulfides can be converted to elemental sulfur. The produced anodic current is expected to be related to: 1) the voltage sweeping rate; 2) the concentration of the polysulfide solution; and 3) the pore size and porosity of the separator.

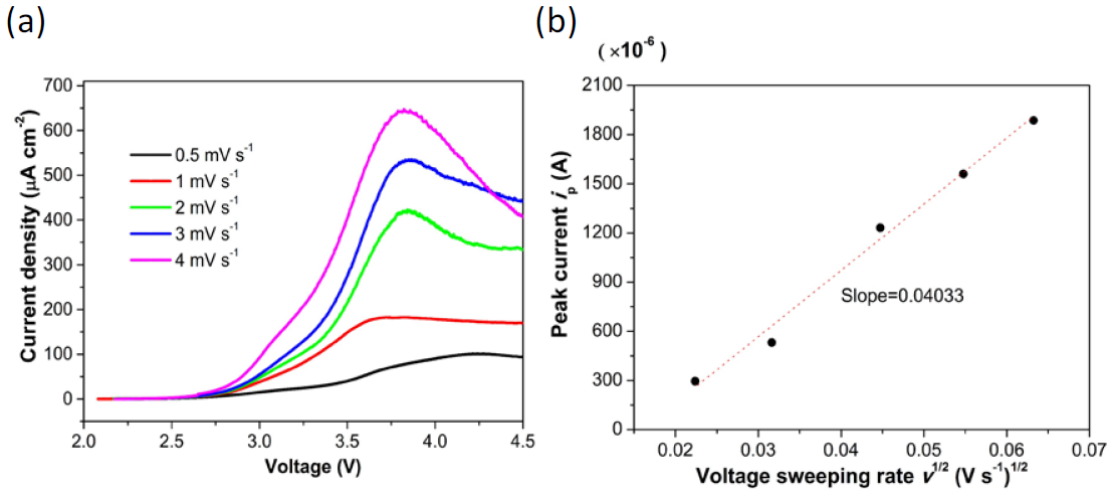

Figure 2.2. (a) Current density-voltage profile of cells with Celgard® 2400 and 0.25 M polysulfide solution at different voltage sweeping rates of 0.5 mV s^{-1}, 1 mV s^{-1}, 2 mV s^{-1}, 3 mV s^{-1}, and 4 mV s^{-1}. (b) The peak current i_p (A) versus square root of voltage sweeping rate $\sqrt{v}$ $(Vs^{-1})^{1/2}$.

Fig. 2.2a shows the anodic current density as a function of the voltage sweeping rate from 0.5 to 4 mV s^{-1}. As the rate increases, the peak current increases. The

currents level off when the rates are 0.5 and 1 mV s^{-1}. As the rate increases to 2 mV s^{-1} and above, a sharp peak current density is observed at about 3.75 V followed by a current decrease. The peak current forms a linear relationship with the square root of the voltage sweeping rate as shown in Fig. 2.2b, meaning the electrochemical oxidation reaction of polysulfide is diffusion controlled. Based on Randles-Sevcik equation (shown below), the apparent diffusion coefficient of polysulfide through the separator can be estimated to be $4.8 * 10^{-8} cm^2\ s^{-1}$. If the porosity of 41% and a tortuosity factor of 3 are considered for the Celgard® PP separator [36], the diffusion coefficient of polysulfide in the DME/DOL electrolyte can be estimated to be $3.5 * 10^{-7} cm^2\ s^{-1}$.

$$i_p = 0.4463nF\sqrt{\frac{nFD}{RT}}AC\sqrt{v} \tag{2.1}$$

Where i_p: the peak current (A), n: the number of electrons (2), F: Faraday constant (96,485 C mol^{-1}), D: the diffusion coefficient ($cm^2\ s^{-1}$) of polysulfide Li_2S_6, R: the gas constant (8.314 J $K^{-1}\ mol^{-1}$), T: temperature (298.15 K), A: the surface area of working electrode (0.97 cm^2), C: the bulk concentration ($2.5 * 10^{-4} mol\ cm^{-3}$), and v: the voltage sweeping rate (V s^{-1}).

Fig. 2.3a compares the anodic current density measured with several polysulfide solutions of different concentration. Higher concentration the polysulfide is, higher the anodic current density is. The peak current density also increases as the concentration of polysulfide increases. The area under the current (A) plot can be integrated as a function of time (s), which is the electrical charge (Coulomb) produced due to the oxidation of polysulfide. For the 0.25 M Li_2S_6 solution, the measured electrical charge is only 0.65 Coulombs, meaning only about a quarter of polysulfides in the solution was oxidized in the LVS measurement. The produced charge can be linearly plotted as a function of the polysulfide concentration which is $\leq$ 0.5 M, as shown in Fig. 2.3b. A linear relationship has also been obtained in the cathodic reaction of polysulfide Li_2S_8 as a function of polysulfide concentration by Dominko et al. [37]. When the polysulfide concentration is as high as 1.0 M, the measured charge obviously deviates

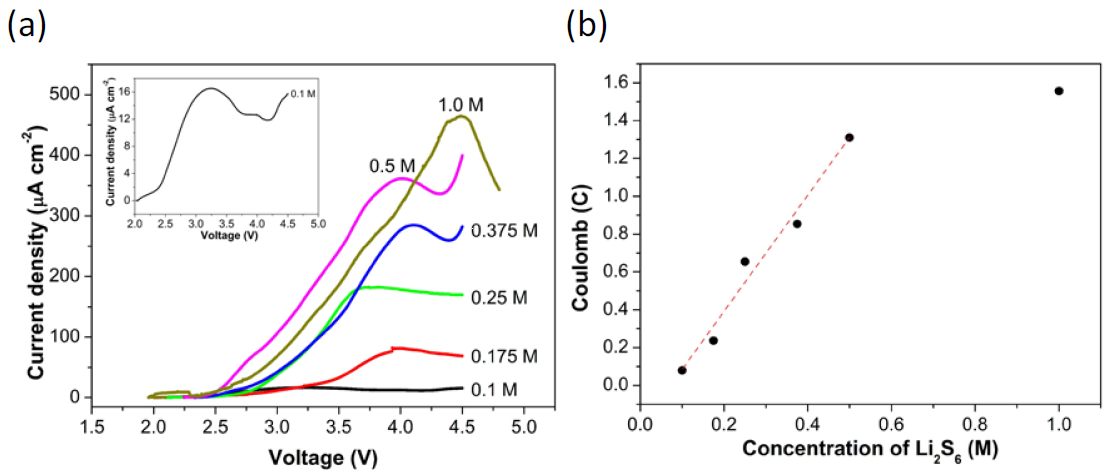

Figure 2.3. (a) Current density-voltage profile of cells with Celgard® 2400 and different polysulfide solutions with concentrations of 0.1 M, 0.175 M, 0.25 M, 0.375 M, 0.5 M, and 1.0 M, the voltage sweeping rate is 1 mV s^{-1}, and the inset figure is a magnified profile for 0.1 M polysulfide solution. (b) The linear relationship of the calculated electrical charge in Coulombs with the concentrations of polysulfide solutions.

from the linear line. In addition, the peak current is generated at a much higher voltage. With high concentration polysulfide, the oxidized solid products which are not conductive will be heavily deposited on the surface of the working electrode, resulting in incomplete oxidation of the polysulfide and significant overpotential.

Fig. 2.4a shows the anodic current densities of various Celgard® separators versus sweeping voltage. For comparison, Celgard® 2400 with blank electrolyte was also evaluated. The cutoff voltage is 4.5 V, at which anodic current slightly increases to 28.4 μA cm^{-2} meaning the electrolyte is still stable without significant decomposition (oxidation). When the polysulfide solution was present in the electrolyte, the current starts to increase significantly at about 2.5 V, which is believed to be solely due to the oxidation of polysulfide. A peak current density of 182 μA cm^{-2} was achieved at about 3.7 V, afterwards the current levels off indicating the transport of polysulfide becomes steady. When Celgard® 2500 was evaluated in the cell, the anodic current follows a similar trend, but with a much higher peak current density of 295 μA cm^{-2}. Celgard® 2500 has a higher porosity and larger pore size than Celgard®

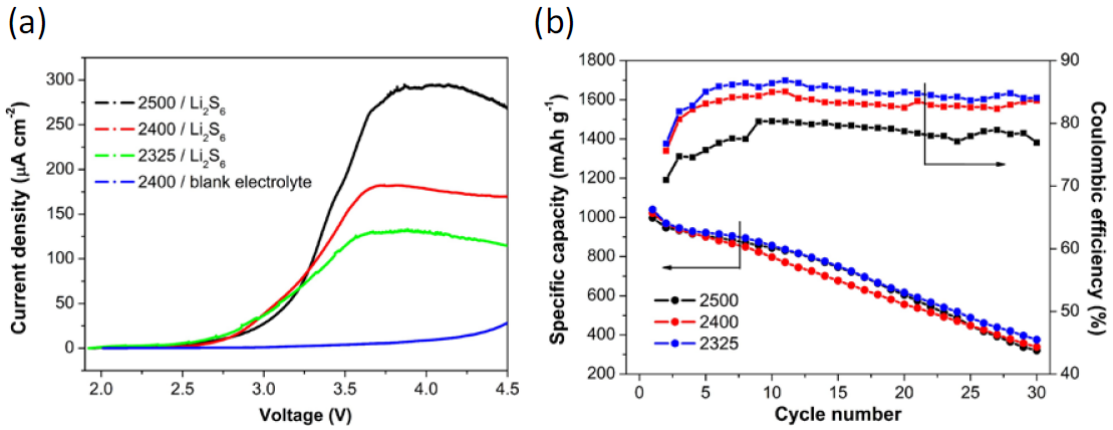

Figure 2.4. (a) Current density-voltage profile of cells with different Celgard® separators (2500, 2400, and 2325) and 0.25 M polysulfide Li_2S_6, and a cell with Celgard® 2400 and blank electrolyte, the voltage sweeping rate is 1 mV s^{-1}. (b) Cycling performance of lithium/dissolved polysulfide cells with these separators at C/5 rate.

2400; therefore the former has a higher anodic current density than the latter. When Celgard® 2325 was evaluated in the cell, the anodic current profile is similar and a low peak current density of 133 μA cm^{-2} was achieved. Celgard® 2325 has a similar porosity as Celgard® 2400 but much smaller pore size, which can reduce the polysulfide transport therefore decrease the anodic current density. These results demonstrate the anodic current due to the oxidation of polysulfide crossed separators is closely related to the porosity and pore size of separators.

To further confirm the relationship between polysulfide transport and separator structure, lithium/dissolved polysulfide cells with these three separators have been evaluated at C/5 rate. The cycling performance with Coulombic efficiency is shown in Fig. 2.4b. Without $LiNO_3$ additive in the electrolyte, the discharge capacities decrease continuously from about 1000 mAh g^{-1} to 300 mAh g^{-1} over 30 cycles because of the continuous loss of active material due to the shuttle of polysulfide, and the Coulombic efficiencies are only in the range of 70-90%. After the first 10 cycles, the cell with Celgard® 2500 shows a faster capacity decrease rate (higher slope) than the other two. After 30 cycles, the cell with Celgard® 2325 retains the highest capacity. As can be seen, the Coulombic efficiencies with these three separators decrease in

the order of Celgard® 2325 > Celgard® 2400 > Celgard® 2500, which is consistent with the order of anodic current densities measured by the LVS method (shown in Fig. 2.4a). If the polysulfide is easy to transport through the separator, shuttle effect would be severe resulting in low capacity over cycles and low Coulombic efficiency.

2.4 Conclusions

In summary, we have successfully developed a new method for evaluating the polysulfide transport through separators by measuring the anodic current density produced by the oxidation of polysulfide under an electric field, which is diffusion controlled. The diffusion coefficient of polysulfide in the DME/DOL electrolyte measured is $3.5 * 10^{-7} cm^2\ s^{-1}$. Within a concentration range ($\leq$0.5 M) of the polysulfide solution, the charge accumulated due to the oxidation of polysulfide is linearly related to the polysulfide concentration. The polysulfide crossover current density can be directly correlated with the porosity and pore size of separators and battery cycling performance. This facile method can be used for quantitative measurement of the polysulfide transport through separators for Li-S battery applications.

3. ENHANCED CYCLABILITY OF LI/POLYSULFIDE BATTERIES BY A POLYMER-MODIFIED CARBON PAPER CURRENT COLLECTOR

3.1 Introduction

To improve the cyclability of Li-S batteries, many approaches, including the development of sulfur-carbon nanocomposites [28,29,38–41], modification of cell component and configuration [42–44], and introducing functional polymers in sulfur cathodes to hold polysulfides [45–51], have been developed. As polysulfides are polar species, functional polymers instead of polytetrafluoroethylene (PTFE) or polyvinylidene fluoride (PVdF) binders can have tremendous benefits for improving the property and performance of sulfur electrodes [52]. For example, alternative binders such as poly(ethylene oxide) (PEO) or poly(acrylic acid) (PAA) have been used in sulfur electrodes and have shown improved cycling performance [53]. Polyvinylpyrrolidone (PVP) has been confirmed to have strong affinity with lithium polysulfides and lithium sulfide, which can improve cycling performance of lithium sulfide electrodes [54]. As lithium polysulfides can be synthesized ex situ and a binder-free carbon paper (CP) current collector can ensure high utilization of sulfur in Li/polysulfide cells, this system can be used as a platform for studying polymer-modified current collectors to correlate the relationship between functional polymers and cell performance.

Herein, we report a study on PVP as a functional polymer in CP current collectors in Li/polysulfide cells. PVP can be dissolved in the electrolyte solvent and exhibits strong affinity with lithium polysulfides, which can reduce the diffusion of polysulfides. The retention of polysulfides in PVP-modified CP collector collectors was evaluated by a linear sweep voltammetry method, which can be used to quantify how much polysulfides are held in the current collectors and linked to the battery

cycling performances. This study demonstrates that functional polymers like PVP are beneficial for Li/polysulfide cells to achieve improved cyclability.

3.2 Experimental

All materials used are included in Table 2.1. All instruments used are included in Table 2.2.

3.2.1 Preparation of Liquid Electrolytes

The blank electrolyte used in this study was prepared by dissolving lithium trifluoromethanesulfonate ($LiCF_3SO_3$, 98%, Acros Organics) in a mixture of dimethoxy ethane (DME, 99+%, Acros Organics) and 1,3-dioxolane (DOL, 99.5%, Acros Organics) (1:1, v/v) by magnetic stirring to render a 1.0 M $LiCF_3SO_3$ solution. Another electrolyte containing lithium nitrate ($LiNO_3$) additive was prepared by dissolving an appropriate amount of $LiNO_3$ (99+%, Acros Organics) in the blank electrolyte to render a 0.1 M $LiNO_3$ solution. To prepare the polysulfide catholyte, stoichiometric amounts of sulfur powder (S, Alfa Aesar) and lithium sulfide (Li_2S, Sigma-Aldrich) were mixed in a proper amount of the blank electrolyte or the electrolyte with $LiNO_3$ additive by magnetic stirring overnight at room temperature to render a 0.25 M Li_2S_6 solution. The electrolyte and polysulfide solution were prepared in an argon-filled glovebox.

3.2.2 Preparation of PVP Solutions

To prepare PVP solution, an appropriate amount of PVP (Mw = 1 300 000, Acros Organics) was dissolved in anhydrous ethanol (200 proof, 99.5%, Sigma-Aldrich) in the glovebox by magnetic stirring at room temperature. Three PVP solutions with different concentrations were prepared and used in this study; they are 0.065, 0.13, and 0.25 wt %.

3.2.3 Modification of Carbon Paper Current Collectors

Commercial binder-free carbon paper (CP) called buckypaper (Buckeye Composites) was used as the current collector in this study. The CP was cut into $\sim$1 cm^2 discs (about 2.0 mg each) and dried at 100 °C for 24 h in a vacuum oven before use. To modify the CP current collector with PVP, a solution filtration method was used. A 50 μL aliquot of PVP solution was added into a CP disc slowly until all the solution was soaked in the paper; then, the disc was dried on a hot plate at 40 °C for 12 h in the glovebox to remove ethanol. The amounts of PVP in the CP are approximately 25, 50, and 100 μg, respectively, for the PVP solutions of 0.065, 0.13, and 0.25 wt %. These three PVP modified CP current collectors are designated as CP-PVP-25, CP-PVP-50, and CP-PVP-100, respectively.

3.2.4 Morphological Characterizations

The morphological characterizations of the CP and CP-PVP current collectors and cycled electrodes were conducted with a JEOL JSM-7800F field emission scanning electron microscope (SEM). The elemental mappings were performed with energy-dispersive X-ray spectroscopy (EDX) attached to the SEM.

3.2.5 Cell Assembly

CR2032 coin cells were used to evaluate the blank CP and CP-PVP current collectors. These cells were assembled in the glovebox. To prepare the control cell, 20 μL of 0.25 M Li_2S_6 polysulfide catholyte (sulfur content: 0.96 mg) was added into a CP current collector, and then a Celgard® 2400 separator was placed on the top of the carbon paper. Next, 20 μL of the blank electrolyte was added on the separator. Finally, the lithium metal anode was placed on the separator. The cell was crimped and taken out of the glovebox for testing. The same cell assembly procedures were used for the CP-PVP current collectors. Some cells were made with the blank elec-

trolyte and polysulfide catholyte without $LiNO_3$ for studying the effect of PVP on cycling performance. The others were made with $LiNO_3$ additive in the electrolyte and polysulfide catholyte for evaluating long cycle life.

3.2.6 Electrochemical Measurements

Linear sweep voltammetry was performed to evaluate polysulfide retention in the blank CP and CP-PVP current collectors. The working principle and cell configuration were described in a previous publication from our group. To prepare the cell, a piece of lithium metal was used as a counter and reference electrode in a homemade Swagelok cell. A piece of blank CP or CP-PVP current collector filled with 0.25 M Li_2S_6 polysulfide solution was placed on the top of a lithium metal reference electrode. A Celgard® 2400 separator was placed on the top of the current collector to separate the carbon paper and working electrode, which is a stainless steel current collector. To minimize the polysulfide consumption due to the reaction with the lithium metal, all cells were tested within 10 min after assembling. The polysulfide in the current collector is in great excess, which can ensure the accuracy of this measurement. Voltage was swept from open-circuit voltage (OCV) to 4.5 V at a scan rate of 1 mV s^{-1} with a Bio-Logic potentiostat. The cells without $LiNO_3$ additive were galvanostatically charged to 3.0 V and discharged to 1.5 V on an Arbin battery cycler with a 5 min rest time between cycles. For the cells with $LiNO_3$ additive, the discharge cutoff voltage was 1.8 V to avoid the reduction of $LiNO_3$. All the cells were tested on the battery cycler without resting to minimize self-discharge. The C-rate used for cycling measurements was based on the mass of sulfur in the polysulfide catholyte in the current collectors (1C = 1672 mA g^{-1}). The specific capacity values shown in this paper are calculated by dividing the capacities obtained by the mass of sulfur. Cyclic voltammetry (CV) was performed on a Bio-Logic VSP potentiostat between 1.5 and 3.0 V at a scanning rate of 0.05 mV s^{-1}. Electrochemical impedance spectroscopy (EIS) data were collected with a Bio-Logic VSP impedance analyzer in the frequency

range of 200 kHz-0.1 Hz on cells which were cycled on the Arbin battery cycler at C/5 in between these tests.

3.3 Results and Discussions

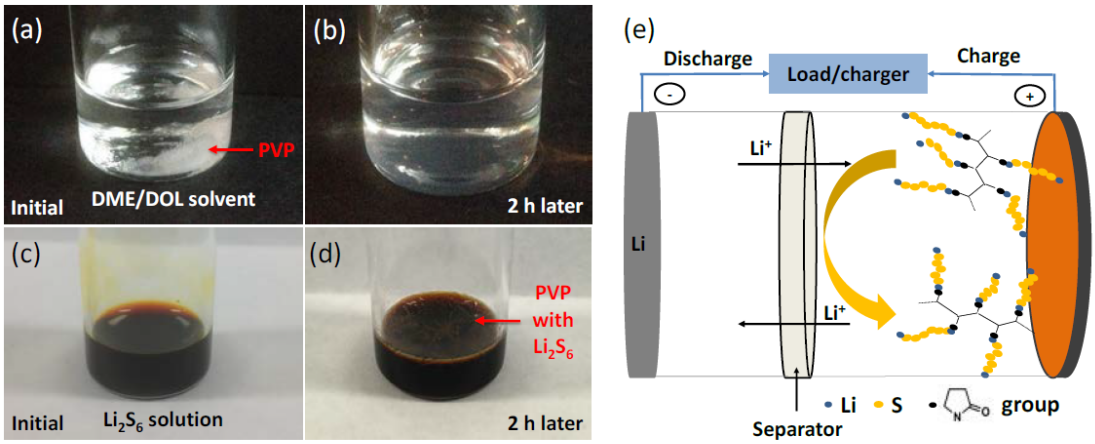

Figure 3.1. (a) Photograph showing PVP powder in the dimethoxy ethane (DME)/1,3-dioxolane (DOL) (1:1 v/v) mixture solvent. (b) Photograph showing PVP completely dissolved in the DME/DOL solvent after 2 h. (c) Photograph of a polysulfide solution of 0.25 M Li_2S_6 in the blank electrolyte. (d) Photograph showing PVP in the polysulfide solution forming separated viscous phases after 2 h. (e) Schematic showing that polysulfides are retained in the CP-PVP current collector in a Li/polysulfide cell.

Fig. 3.1 shows the assessment of PVP's solubility in the electrolyte solvent and polysulfide solution. At initial, an appropriate amount of PVP powder was added in the DME/DOL (1:1 v/v) mixture solvent, as shown in Fig. 3.1a. Two hours later, the PVP was completely dissolved in the solvent, forming a homogeneous solution, as shown in Fig. 3.1b. This solution is transparent, and the viscosity is slightly increased. Fig. 3.1c shows a polysulfide solution of 0.25 M Li_2S_6 in the blank electrolyte. After PVP was added in the polysulfide solution, floccules with separated viscous phases were formed, as shown in Fig. 3.1d. This phenomenon indicates that PVP could form complexes with lithium polysulfides due to the affinity between them, which

can increase viscosity and reduce flowability of the polysulfide solution. This result led to the study of PVP-modified CP current collectors in Li/polysulfide cells. The schematic in Fig. 3.1e depicts the interaction between PVP and lithium polysulfides, which can enhance the retention of polysulfides in the current collector and reduce the shuttle of polysulfides to the lithium metal anode in a Li/polysulfide cell.

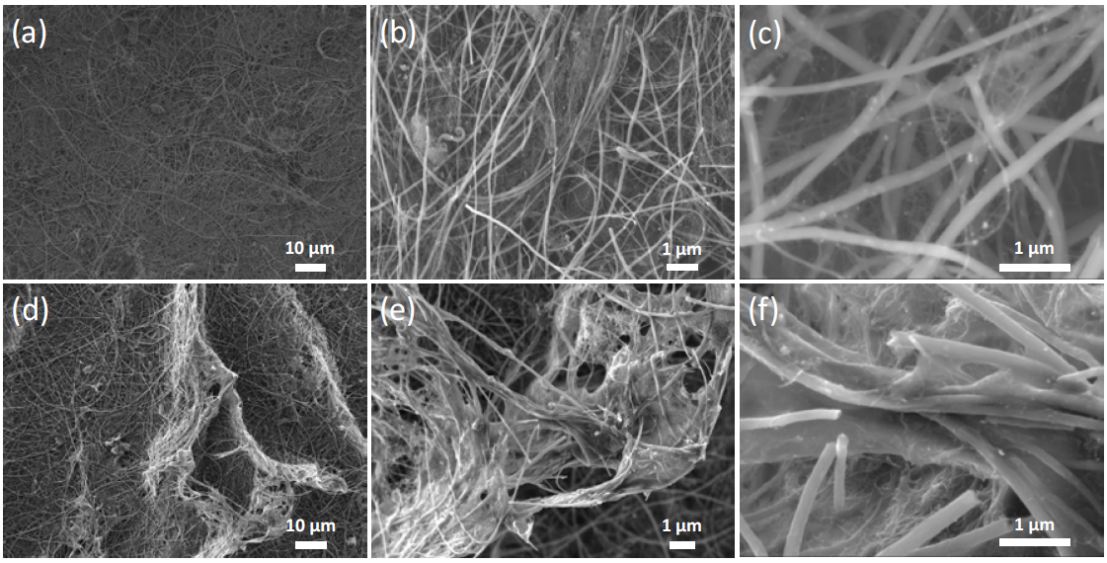

Figure 3.2. (a-c) SEM images of the blank CP current collector. (d-f) SEM images of the CP-PVP-50 current collector.

The morphology of the blank CP and CP-PVP current collectors was examined by SEM, as shown in Fig. 3.2. It can be seen that the blank CP current collector has a flat surface, which is made of weaving carbon nanotubes (CNTs) and carbon nanofibers (CNFs), as shown in Fig. 3.2 (a-c). The ultralong length and curved shape of CNFs enable the freestanding characteristic of the CP current collector. The large voids between CNTs and CNFs provide space for holding additional polymers and polysulfide catholyte. After a small amount (1.2-5.0 wt %) of PVP was added into the CP current collector by the solution filtration process, the surface becomes uneven, as shown in Fig. 3.2d, which is due to the evaporation of ethanol. The magnified SEM images clearly show the presence of PVP within the CNT/CNF network, as shown in Fig. 3.2 (e, f). This long chain polymer with an M_w of ~1 300 000 acts as a glue

bonding the CNTs and CNFs and fills some space among them. The PVP in the CP current collector changes the inner porosity and morphology, therefore affecting its affinity with lithium polysulfides.

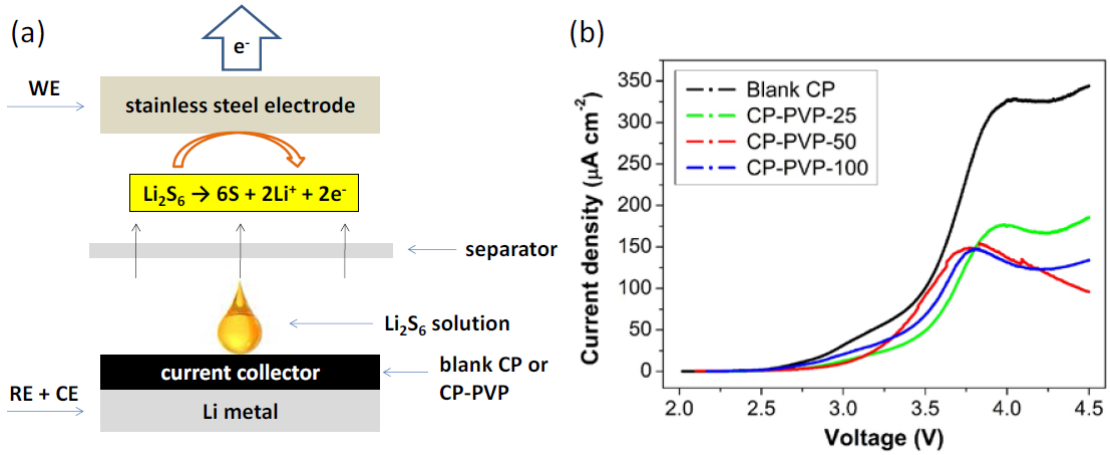

Figure 3.3. (a) Schematic of the experimental cell and working principle of the linear sweep voltammetry method for the evaluation of polysulfide retention in the blank CP or CP-PVP current collector, which is a reservoir for the polysulfide solution in the experiment. (b) Current densityvoltage profile of cells with the blank CP, CP-PVP-25, CP-PVP-50, CP-PVP-100 current collectors.

To evaluate the retention of polysulfides in the CP-PVP current collector, linear sweep voltammetry was performed on a designed cell, as shown in Fig. 3.3a. This experiment can be used to evaluate the transport of polysulfides through separators, and it also can be used to evaluate the affinity property of CP current collectors to lithium polysulfides. Under an increasing sweeping potential, polysulfide anions can diffuse out of the CP current collector, migrate through the separator, and get oxidized on the working electrode to produce an anodic current, which can be measured by the potentiostat. The current measured is strongly related to the separator structure, polysulfide solution, and current collector [55]. Fig. 3.3b shows the oxidation current density as a function of sweeping potential obtained with the blank CP and CP-PVP current collectors. The sweeping potential starts at OCV and ends at 4.5 V. Polysulfides are oxidized when the potential is above 2.5 V. The current density measured with the blank CP current collector increases significantly and reaches

a peak at 325 μA cm^{-2} and then levels off, which indicates that the oxidation of polysuflides migrated through the separator is stabilized. In contrast, the current density peaks with the CP-PVP current collectors are only half of the former. The affinity between PVP and lithium polysulfides significantly enhances the retention of polysulfides in the CP-PVP current collector, reducing the oxidation current measured. With various amounts of PVP in the CP current collector, the current profile is similar. The charge in coulombs due to the oxidation of polysulfides is proportional to the area under the current curves. The areas of all CP-PVP current collectors under the curves are approximately 50% of that of the blank CP current collector, indicating that almost half the lithium polysulfides are retained in the paper due to the presence of PVP. This result demonstrates that PVP can help retain polysulfides in the CP-PVP current collectors. The CP-PVP-25 shows a slightly higher current and larger area under the curve than those of the CP-PVP-50 and CP-PVP-100. In contrast, the current obtained with the CP-PVP-50 is quite similar to that obtained with the CP-PVP-100. This means that only 50 μg of PVP is sufficient for holding most lithium polysulfides in this case.

The cell performance of the control cell with the blank CP current collector and those with CP-PVP current collectors are compared in Fig. 3.4a. It can be seen that the control cell shows a high initial discharge capacity of 1100 mAh g^{-1}, but a continuous decrease to 200 mAh g^{-1} after 36 cycles. The Coulombic efficiency shown in Fig. 3.4b follows an increase-then-decrease trend and ends at 60% after 36 cycles. The large voids in the CP paper cannot hold polysulfides, resulting in continuous loss of active material in the cathode. The capacity fade also results from the degradation of the lithium metal anode due to polysulfide corrosion. Without $LiNO_3$ additive in the electrolyte, the Coulombic efficiency is low due to the severe shuttle effect and continuous reduction of polysulfide on the lithium metal anode [25]. With 25 μg PVP in the CP current collector, the cell shows a high initial capacity of over 1100 mAh g^{-1} and relatively stable capacities over 20 cycles, followed by a significant capacity fade. The initial high capacities are enabled by the presence of PVP in the

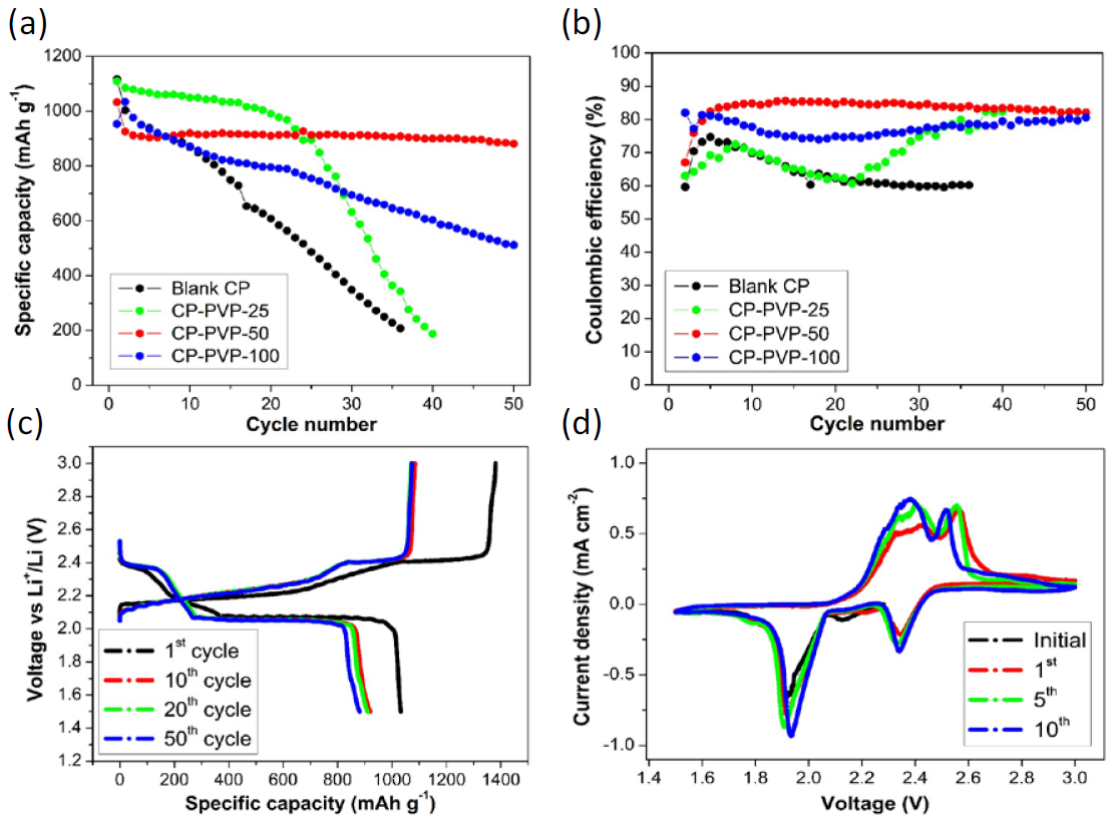

Figure 3.4. (a) Cyclability and (b) Coulombic efficiency of the cells with the blank CP and CP-PVP current collectors without $LiNO_3$ additive in the electrolyte at C/10 rate. (c) Voltage vs specific discharge capacity profiles of the 1^{st}, 10^{th}, 20^{th}, and 50^{th} cycles of the cell with the CP-PVP-50 current collector at C/10 rate. (d) Cyclic voltammograms of the cell with the CP-PVP-50 current collector at a potential sweep rate of 0.05 mV s^{-1} between 1.5 and 3.0 V.

CP current collector. Over cycles, PVP cannot hold polysulfides anymore due to repeated deposition of insoluble sulfur and lithium sulfide, which could move PVP to dead spots in the current collector. When the PVP content increases to 50 μg, the cell shows an initial capacity of 1030 mAh g^{-1} and a stable capacity of over 900 mAh g^{-1} from the 2^{nd} to the 50^{th} cycle. When the PVP content further increases to 100 μg, the cell shows a continuous decrease in the cycling profile, but it is still much better than the control cell. With too much PVP in the CP current collector, the conductivity of the current collector would decrease and the viscosity of the polysulfide catholyte would increase, which can affect the electrochemical reversibility of sulfur. All the

cells with CP-PVP current collectors show higher capacities than the control cell. In addition, the Coulombic efficiencies of these cells are higher than that of the control cell. These results demonstrate that the PVP in the CP current collector can improve the utilization of sulfur in Li/dissolved polysulfide cells, retention of polysulfide in the cathode, and Coulombic efficiency. The content of PVP can affect the complexes formed in the polysulfide catholyte, as shown in Fig. 3.1d. More PVP would result in better retention of polysulfides in the electrode. However, dissolved PVP also changes the viscosity of electrolyte and conductivity in the current collector, which can affect the utilization of sulfur. An optimized content of 50 μg of PVP in this case leads to a good balance between the performance and affinity property of the CP current collector.

Fig. 3.4c shows the voltage profile of the 1^{st}, 10^{th}, 20^{th}, and 50^{th} cycles of the cell with the CP-PVP-50. The cell can be discharged to 1.5 V since no $LiNO_3$ reduction occurs at low potential ($\leq$1.65 V). With the presence of PVP in the current collector forming complexes with polysulfides, the retention of polysulfides in the electrode is significantly enhanced; therefore, the shuttle effect can be suppressed, which can be evidenced from the improved cycling stability. The charge and discharge plateaus are very close to each other except for the 1^{st} cycle, which indicates that PVP can be an efficient binder for holding polysulfides from rapid diffusion and loss from the cathode. In addition, no increased overpotential is observed over 50 cycles. The significant capacity decrease after the 1^{st} cycle could be because the PVP-modified current collector has to optimize itself when the cathode reactions occur. After self-optimization, the current collector reached stability, leading to stable cycle life. Fig. 3.4d shows the cyclic voltammogram (CV) of the cell with the CP-PVP-50. There are two cathodic peaks at 2.35 and 1.95 V corresponding to the reduction reactions of sulfur to low-order polysulfides and low-order polysulfides to Li_2S, and two distinguishable anodic peaks at 2.35 and 2.45 V, which indicate the transition of Li_2S to high-order polysulfides/sulfur [35]. The cell exhibits a stable CV profile over 10 cycles without decay of peak intensity.

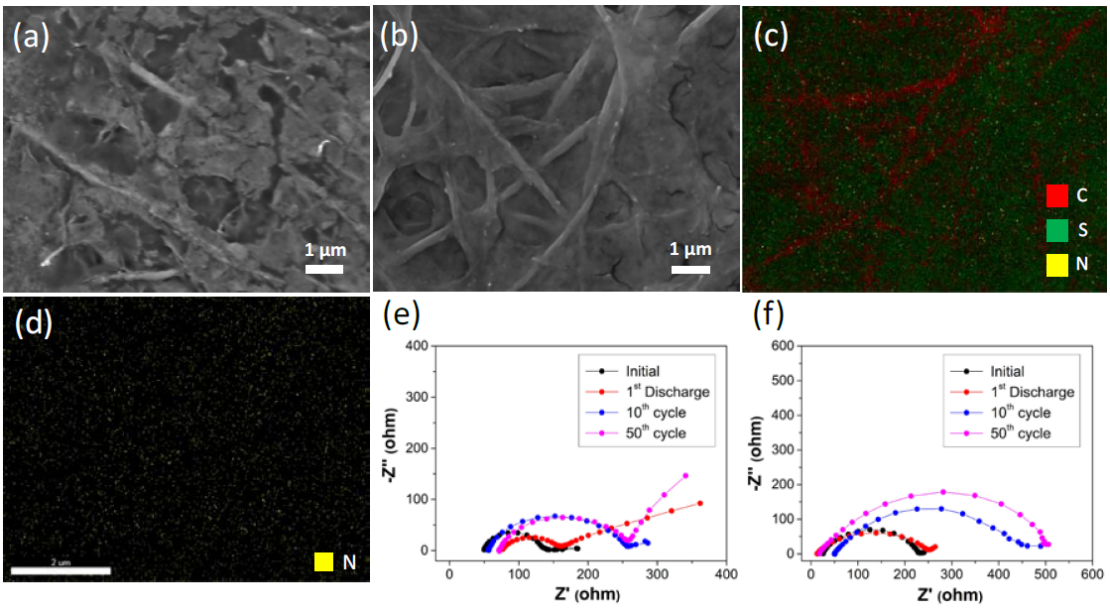

Figure 3.5. (a) SEM image of the blank CP current collector after 5 cycles. (b) SEM image of the CP-PVP-50 current collector after 5 cycles. (c) EDX elemental mapping of SEM image in (b). (d) Nitrogen elemental mapping of the SEM image in (b). (e) Nyquist plots of the control cell with the blank CP current collector after different cycles. (f) Nyquist plots of a cell with the CP-PVP-50 current collector after different cycles.

Fig. 3.5 (a, b) shows the morphology of two cycled electrodes: one is the electrode with the blank CP current collector (Fig. 3.5a), and the other one is with the CP-PVP-50 (Fig. 3.5b). After 5 cycles, the electrode with the blank CP current collector shows many cracks, which are due to the repeated formation of charged and discharge products resulting in significant volume change. The blank CP cannot hold the active material and electrolyte together upon cycling. In contrast, the electrode with the CP-PVP-50 shows a very uniform morphology without cracks after 5 cycles. The CP current collector is uniformly filled and covered with discharged products and electrolyte. The EDX analysis shows that the sulfur element in lithium sulfide and lithium salt is uniformly distributed in the pores of the CP paper, as shown in Fig. 3.5c. A small amount of nitrogen element can also be detected, as shown in Fig. 3.5d, which can be only from the PVP since no $LiNO_3$ additive was added in the

polysulfide catholyte. It can be seen that PVP is also uniformly distributed across the electrode. The electrolytesoluble PVP molecules can dynamically change their morphology to stabilize the electrode upon cycling, which is beneficial for maintaining a stable electrode in Li-S batteries.

Fig. 3.5 (e, f) compares the Nyquist plots of two cells with the blank CP and CP-PVP-50 current collectors. The impedances were measured after different cycles. The intercepts of Nyquist plots in the high-frequency regions are attributed to the bulk resistance of the liquid electrolyte, and the semicircles in the high-medium frequency regions are charge transfer resistances of the electrode/electrolyte interfaces. The linear segment in the low-frequency region corresponds to the diffusion limitation within the electrodes. It can be seen that the cell with the CP-PVP-50 has a lower bulk resistance (26 ohms) but higher charge transfer resistance (206 ohms) than the cell with the blank CP current collector before cycling. PVP can hold polysulfides in the cathode side and reduce diffusion of polysulfides into the bulk electrolyte between the cathode and lithium metal anode, which helps maintain a low bulk resistance. However, its insulating property makes the charge transfer difficult at the electrode/electrolyte interface. After the 1^{st} and 50^{th} cycles, the bulk resistance slightly decreases when the CP-PVP-50 was used in the cell, whereas the bulk resistance significantly increases when the blank CP current collector was in the cell. After the 50^{th} cycle, the charge transfer resistance increases from 94 to 186 ohms in the cell with the blank CP current collector and from 206 to 483 ohms in the cell with the CP-PVP-50.

To further improve the cycling performance, the CP-PVP-50 was tested with the electrolyte containing $LiNO_3$ additive, which can show a synergistic benefit. Fig. 3.6a shows the cycling performance of the cell. A high initial discharge capacity of over 1300 mAh g^{-1} and a reversible capacity of 1200 mAh g^{-1} in the first 20 cycles were obtained. Afterward, the cell maintains an average capacity of about 1000 mAh g^{-1} for 80 cycles. The Coulombic efficiency is 95-99%. With $LiNO_3$ additive in the electrolyte, the lithium metal anode is passivated, which stops aggressive reduction

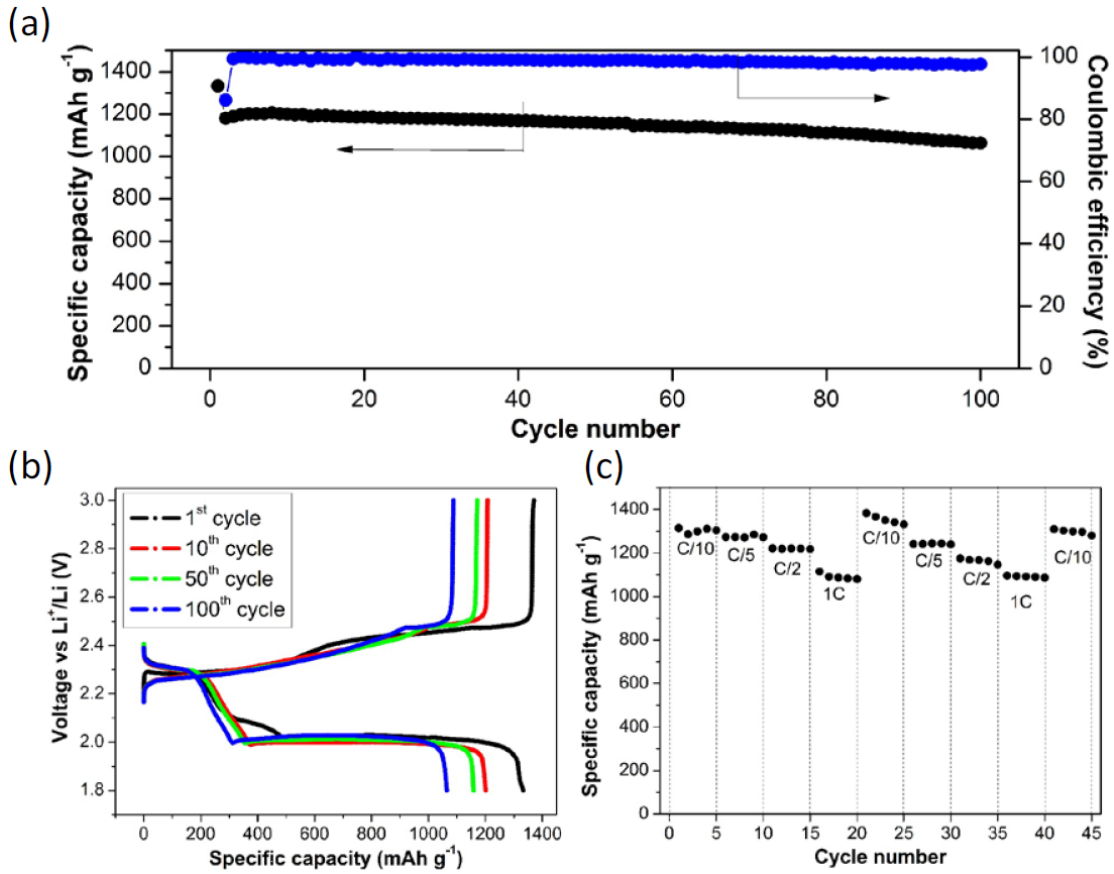

Figure 3.6. (a) Cyclability and Coulombic efficiency of the cell with the CP-PVP-50 current collector and 0.1 M $LiNO_3$ additive in the electrolyte at C/5 rate. (b) Voltage vs specific discharge capacity profiles of the 1^{st}, 10^{th}, 50^{th}, and 100^{th} cycles of the cell. (c) Cyclability of the cell at C/10, C/5, C/2, and 1C rates. The capacity values are in terms of the sulfur mass in the Li_2S_6 solution.

of polysulfides, therefore improving capacity retention and Coulombic efficiency [56]. Fig. 3.6b indicates the voltage profile of the 1^{st}, 10^{th}, 50^{th}, and 100^{th} cycles. After 100 cycles, the capacity is over 1000 mAh g^{-1} on the voltage profile. During the first 100 cycles, the capacity fade is only 0.25% per cycle and the voltage plateaus are relatively stable. The rate capability of the cell is shown in Fig. 3.6c. A specific capacity of about 1300 mAh g^{-1} is achieved at C/10, and a specific capacity of 1250 mAh g^{-1} is achieved at C/5 rate. The specific capacity is around 1200 mAh g^{-1} at C/2 and 1100 mAh g^{-1} at 1C rate, respectively. When the rate was switched back to C/10 rate after 1C rate, the capacity is a little higher than that before. The

slight capacity decay observed during the cycling is not permanent. After multiple C rate tests, the capacity at C/10 rate in the 3^{rd} cycle is back to the high capacity level of more than 1200 mAh g^{-1}. These results show the good rate capability and reversibility of cells enabled by the PVP-modified CP current collectors with $LiNO_3$ additive in the electrolyte.

3.4 Conclusions

In summary, we have studied PVP-modified CP current collectors in Li/polysulfide cells. PVP is soluble in the electrolyte solvent, but it can form complexes with lithium polysulfides because of the affinity between them, which can improve the retention of polysulfides in the current collector. About 50% of lithium polysulfide Li_2S_6 can be retained in the CP-PVP current collectors when only 50 μg of PVP was used, which is measured by the linear sweep voltammetry method. The PVP-modified CP current collectors can increase utilization of sulfur and Coulombic efficiency, enhance cycling stability, and maintain integrity of the electrode. Although PVP can increase charge transfer resistance in the cell due to its insulating property, it can help maintain a low bulk resistance by preventing polysulfides in the cathode from diffusing into the blank electrolyte. When the CP-PVP current collector worked with electrolyte containing $LiNO_3$ additive, a high reversible capacity of over 1000 mAh g^{-1} with a high Coulombic efficiency of close to 100% was achieved at C/5 rate for 100 cycles. This study demonstrates that functional polymers like PVP can optimize the property of CP current collectors, which can lead to improved cycling stability in Li/polysulfide cells.

4. A BINDER-FREE SULFUR/CARBON COMPOSITE ELECTRODE PREPARED BY SULFUR SUBLIMATION METHOD FOR LI-S BATTERIES

4.1 Introduction

The conventional method of making sulfur electrodes by mixing sulfur powder, carbon, and polymer binder is inappropriate for making uniform and high performance electrodes. Poor contact between large sulfur particles and carbon results in low utilization and inhomogeneous distribution of current upon cycling [29,52]. To overcome these issues, many approaches including the synthesis of sulfur-carbon nanocomposites [47, 57–60], fabrication of novel cathode and cell configurations [14, 61, 62], and making polysulfide-blocking separators have been developed [63]. The primary methods for making sulfur-carbon nanocomposites are (i) heat treatment and (ii) solution-based synthesis. The heat treatment method is to impregnate a micro or mesoporous carbon matrix with melted sulfur, which can result in nanoscaled sulfur in the carbon matrix. The solution-based synthesis is to precipitate sulfur particles in solution through a heterogeneous nucleation reaction, which tends to form larger sulfur particles.

Sulfur can sublime at elevated temperature. Hagen et al. sublimed sulfur into a vertical-aligned carbon nanotube (CNT) substrate [64]. Fu et al. sublimed sulfur into a CNT paper current collector using Argon as a carrier gas [65]. Herein, we present a study on a binder-free sulfur/carbon composite electrode prepared by the sulfur sublimation method in air. At certain temperature and air flow rate, sulfur can be melted and vaporized. Solid sulfur nanoparticles can be deposited into commercial binder-free carbon paper which also acts as a current collector in batteries. Compared with the other methods for making sulfur/carbon composite electrodes, this method has several advantages. Firstly, it is a green, solvent-free method and the sulfur

powder undergoes a physical deposition process maintaining its intrinsic composition. Secondly, the sulfur vapor can infiltrate large pores in the carbon paper forming intimate contact with carbon. Finally, it is scalable and provides another synthesis route for making high performance sulfur-carbon composite electrodes.

4.2 Experimental

All materials used are included in Table 2.1. All instruments used are included in Table 2.2.

4.2.1 Preparation of Sulfur/Carbon Composite Electrodes

Commercial binder-free carbon paper called buckypaper (Buckeye Composites) was used as a support for sulfur and the current collector in this study. To prepare the composite electrode, 1.5 g of sulfur powder (Fisher Scientific) was uniformly loaded in a 20 mL beaker. A disc of carbon paper ($\sim 10\ cm^2$) was put on top of the beaker. The beaker was heated at about 200 °C on a hot plate. The whole setup was installed in a fume hood with constant air flow (55 ft/min) to enhance sulfur vapor infiltration. The sulfur powder was fully melted into liquid phase and sulfur vapor with white/yellow mixed color went into the carbon paper. Four deposition times, which are 2, 4, 8, and 15 minutes, were applied for making these electrodes which are designated as SE-2, SE-4, SE-8 and SE-15, respectively. Finally the prepared electrode was cut into $\sim 1\ cm^2$ discs, each contains 1.9 mg carbon.

4.2.2 Preparation of Liquid Electrolytes

The blank electrolyte used in this study was prepared by dissolving lithium bis (trifluoromethane) sulfonimide (LiTFSI, 98%, Acros Organics) in a mixture of dimethoxy ethane (DME, 99+%, Acros Organics) and 1,3-dioxolane (DOL, 99.5%, Sigma Aldrich) (1:1, v/v) by magnetic stirring to render 1.0 M LiTFSI solution. Another electrolyte

containing lithium nitrate ($LiNO_3$) additive was prepared by dissolving an appropriate amount of $LiNO_3$ (99+%, Acros Organics) in the blank electrolyte to render 1.0 M LiTFSI/0.1 M $LiNO_3$ solution. The electrolytes were prepared in an Argon-filled glove box.

4.2.3 Morphological Characterizations

The morphological characterizations of the electrodes were conducted with a JEOL JSM-7800F field emission scanning electron microscopy (SEM). X-Ray Diffraction (XRD) patterns were recorded by using Cu-Kα radiation at 50 kV with an X-ray diffractometer (D8 Discover A25, Bruker AXS). N_2 sorption/desorption measurement was carried out on a Quantachrome Autosorb iQ gas sorption analyzer, and the pore size distribution was calculated based on the NLDFT model assuming a slit-shape pore structure.

4.2.4 Cell Assembly

CR2032 coin cells were used and assembled in the Argon-filled glove box to evaluate the electrochemical performance of as-prepared electrodes. To prepare the cells, 20 μL of the electrolyte was added into an electrode, and then a Celgard® 2400 separator was placed on top of the electrode. Another 20 μL of the electrolyte was added on the separator. Finally, the lithium metal anode was placed on the separator. The cell was crimped and taken out of the glove box for testing. Cells with the blank electrolyte were made for the measurement of cyclic voltammetry. Cells with $LiNO_3$ additive in the electrolyte were made for evaluating cycle life.

4.2.5 Electrochemical Measurements

Cells were galvanostatically discharged to 1.7 V and charged to 2.8 V on an Arbin battery cycler with 5-minute rest time between cycles. All cells were tested immedi-

ately after they were made. The C-rate used for cycling measurements was based on the mass of sulfur in the electrode (1C = 1,672 mA g^{-1}). The specific capacity values shown in this paper are calculated by dividing the capacities obtained by the mass of sulfur. Cyclic voltammetry was performed on a Bio-Logic VSP potentiostat between 1.5 V and 3.0 V at a scanning rate of 0.05 mV s^{-1}.

4.3 Results and Discussions

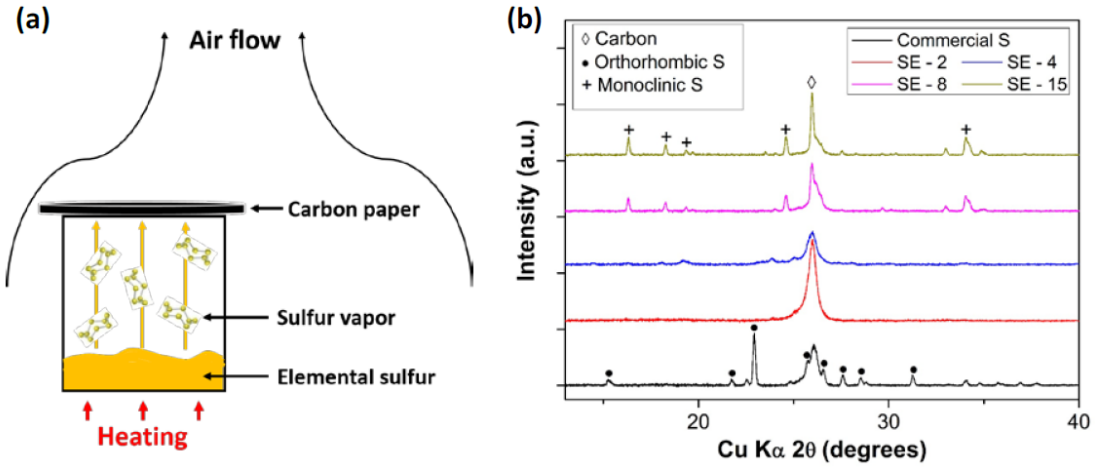

Figure 4.1. (a) Schematic illustration of the experimental process for making a binder-free sulfur/carbon composite electrode by the sulfur sublimation method. (b) XRD patterns of the sulfur/carbon composite electrodes SE-2, SE-4, SE-8, and SE-15, and the control sample of commercial sulfur on carbon paper.

Fig. 4.1a shows the experimental setup in a fume hood with constant air flow. To prepare the composite electrode, sulfur powder was uniformly loaded in a beaker. A disc of carbon paper was put on top of the beaker. The beaker was heated at about 200 °C, at which sulfur vapor can be formed modestly and continuously. When the sulfur is vaporized, individual sulfur rings or sulfur clusters are small enough to penetrate small pores and get deposited in the carbon matrix. The air flow enhances sulfur infiltration in the carbon paper. This process helps break down large sulfur particles into small ones which are beneficial for achieving high utilization of sulfur in batteries. Under these conditions, desirable sulfur contents can be obtained within

15 min. Four deposition times (i.e., 2, 4, 8, and 15 min) resulted in sulfur loading of approximately 0.4, 0.9, 1.7, and 2.8 mg cm^{-2}, and these electrodes are designated as SE-2, SE-4, SE-8 and SE-15, respectively. The prepared electrode was cut into ∼1 cm^2 discs, each contains 1.9 mg carbon.

X-Ray Diffraction (XRD) was used to qualitatively analyze the sulfur crystal structure formed in the electrodes. For comparison, commercial sulfur on a piece of carbon paper was also examined by XRD. Fig. 4.1b shows the XRD patterns in the 2θ range between 13° and 40° wherein the characteristic peaks of sulfur and carbon can be seen. The main peak at 26.0° is a characteristic peak of (002) crystal plane of carbon nanotubes [66]. The commercial sulfur powder on the carbon paper shows peaks that are matched with the XRD pattern of the orthorhombic sulfur [67,68]. The SE-2 does not show any peaks of sulfur besides the carbon peak, indicating a small amount of sulfur was deposited in the sample. The SE-4 shows a few peaks, but they cannot be assigned to either orthorhombic crystal or monoclinic crystal structure. When the deposition time increases to 8 and 15 min, several major peaks of monoclinic sulfur crystal can be seen along with few small unknown peaks. It is reported that sulfur undergoes a phase transition from the orthorhombic to monoclinic structure when the temperature is 200 °C [67, 69]. Vaporized sulfur rings re-stack into the favorite monoclinic crystal structure that is stable at elevated temperature [67]. The monoclinic sulfur may transition to other structures, e.g., orthorhombic structure, over a long period of time, but it is not interest of this work.

The morphology of the sulfur/carbon composite electrode was examined by SEM, as shown in Fig. 4.2a. Such carbon paper has been used in Li/polysulfide batteries as it can hold polysulfide solution and cycled products [35]. It can be seen that a lot of irregular sulfur particles were deposited in the voids of the carbon paper. Some sulfur particles are large, which are in the range of a few microns. Overall, it is a uniform composite electrode. The magnified SEM image in the inset picture shows that the large sulfur particles are in the form of many nanoparticles filling all space between carbon nanofibers and nanotubes. The SEM results show that this sulfur

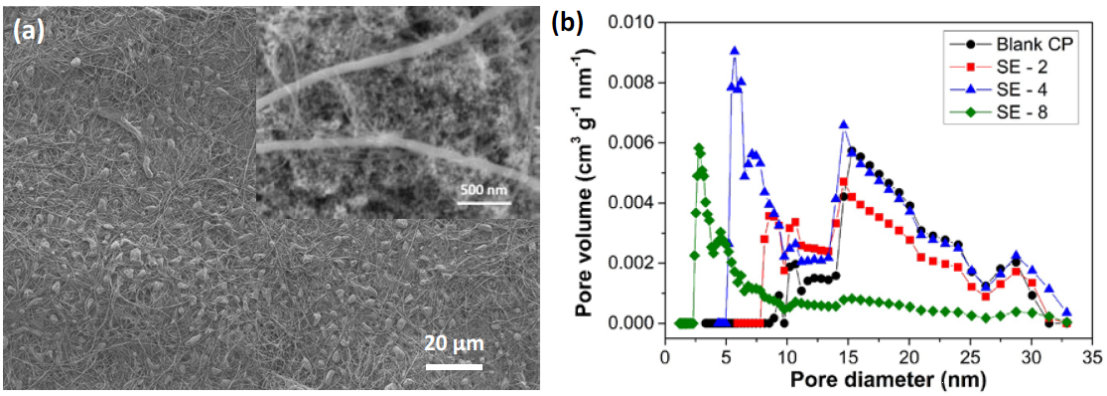

Figure 4.2. (a) SEM image of a prepared electrode, the inset figure is a magnified SEM image showing sulfur nanoparticles formed within voids of the carbon paper. (b) Pore size distribution of the blank carbon paper (CP), SE-2, SE-4, and SE-8.

sublimation method can facilitate breaking down large sulfur particles and dispersing sulfur nanoparticles into a carbon matrix. These sulfur nanoparticles would have good contact with carbon in the electrode, which can improve the ion and electron transport within the composite electrode in batteries.

Fig. 4.2b shows the pore size distribution within the blank carbon paper and composite electrodes. In the blank carbon paper, a broad pore size in the range of 8 - 33 nm is observed. The carbon paper consists of thin carbon nanotubes and thick carbon nanofibers as seen in the SEM image in Fig. 4.2a forming a variety of pores among them. As sulfur nanoparticles are formed in the carbon paper, the volume of large pores starts to decrease and smaller pores start to appear. For example, the SE-4 has a significant volume of pores with a diameter centered at about 7 nm which is smaller than all pores in the blank carbon paper and SE-2. In contrast, the SE-8 only shows a volume of pores with a diameter centered at about 3 nm and almost all pores between 8 - 33 nm are gone. The small pores in the SE-4 and 8 can only be formed between or within the newly formed sulfur nanoparticles, which filled all large pores in the carbon paper as seen in Fig. 4.2a.

The SE electrodes exhibited different cycling behaviour, as shown in Fig. 4.3a. The SE-2 and SE-4 show higher discharge capacities and better cycling stability than

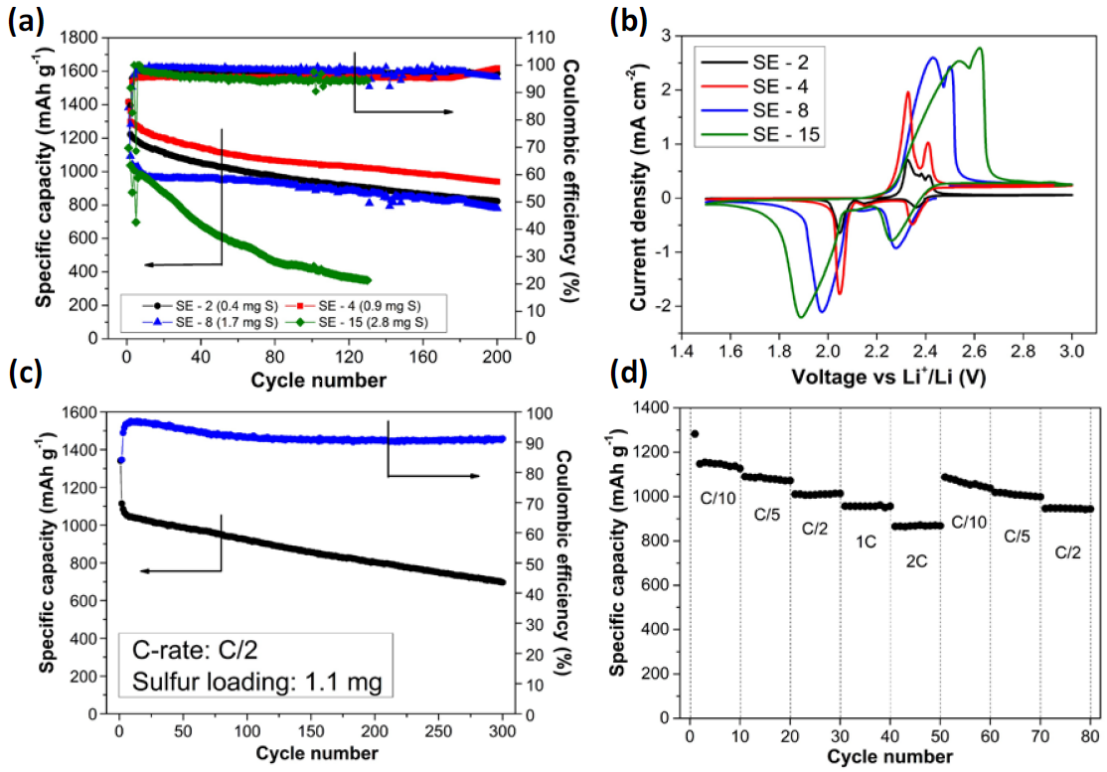

Figure 4.3. (a) Cyclability and Coulombic efficiency of the cells with SE-2, SE-4, SE-8, and SE-15 electrodes at C/5 rate. (b) The 1^{st} cyclic voltammograms of the cells without $LiNO_3$ additive in the electrolyte at a potential sweep rate of 0.05 mV s^{-1} between 1.5 and 3.0 V. (c) Cyclability and Coulombic efficiency of the electrode with sulfur loading of 1.1 mg cm^{-2} at C/2 rate. (d) Rate capability of the cell used in (c).

the SE-8 and SE-15 due to the low sulfur contents. The initial discharge capacity of the SE-2 and SE-4 can be as high as ~1,400 mAh g^{-1}, in contrast to ~1,100 mAh g^{-1} of the SE-8 and SE-15. The SE-2, SE-4, and SE-8 maintain a high reversible capacity of 850, 1000, and 820 mAh g^{-1} after 200 cycles, respectively; however, the SE-15 shows continuous capacity decay to 300 mAh g^{-1} after 120 cycles. The long sublimation time (15 min) results in high sulfur loading (2.8 mg cm^{-2}) in the SE-15. The formed sulfur particles are very large in the electrode, which result in low utilization of sulfur and fast capacity fade. All cells show a high Coulombic efficiency of >95% during cycling.

Fig. 4.3b shows the 1^{st} cyclic voltammograms (CV) of cells with these electrodes. All cells show two typical cathodic peaks representing the reduction reactions of sulfur to low-order polysulfides and low-order polysulfides to Li_2S. As the sulfur loading increases, the peak shifts to lower potential and the peak area increases. Similarly, all cells show distinguishable anodic peaks which represent the reverse oxidation of Li_2S to high-order polysulfides/sulfur. Due to the high sulfur contents in the SE-8 and SE-15, the anodic peaks are much broader and higher than those in the SE-2 and SE-4. In addition, the 2^{nd} anodic peak at high potential increases more significantly than the 1^{st} anodic peak at low potential as the sulfur content increases. This indicates slower electrode kinetics and more incomplete conversion of active material to elemental sulfur in the anodic sweep as the sulfur content is higher.

To further evaluate long cycle life, an electrode with sulfur loading of 1.1 mg cm^{-2} was cycled for 300 cycles at C/2 rate, as shown in Fig. 4.3c. A high initial discharge capacity of over 1,300 mAh g^{-1} and a reversible capacity of 1,000 mAh g^{-1} in the first 50 cycles were obtained. Afterwards, the cell maintains a reversible capacity of about 700 mAh g^{-1} after 300 cycles. The capacity fade is only 0.17% per cycle and the voltage plateaus are relatively stable (not shown). The Coulombic efficiency is over 90%. With $LiNO_3$ additive in the electrolyte, lithium metal anode was passivated which stops aggressive reduction of polysulfides, therefore improves capacity retention and Coulombic efficiency [25,56]. The rate capability of the cell is shown in Fig. 4.3d. A specific capacity of about 1,300 mAh g^{-1} is achieved in the 1^{st} cycle at C/10 rate and is stable at 1,150 mAh g^{-1} after 10 cycles. A reversible capacity of 1,100 mAh g^{-1} is achieved at C/5 rate. The specific capacity is around 1,000, 950, and 850 mAh g^{-1} at C/2, 1C, and 2C rate, respectively. When the rate was switched back to C/10 rate after 2C rate, the capacity went back to 1,100 mAh g^{-1}. At C/5 and C/2 rates, the specific capacities are quite similar as those obtained before the rate testing cycle. These results show the good reversibility and rate capability of the cells enabled by the sulfur nanoparticles deposited in the carbon paper electrodes.

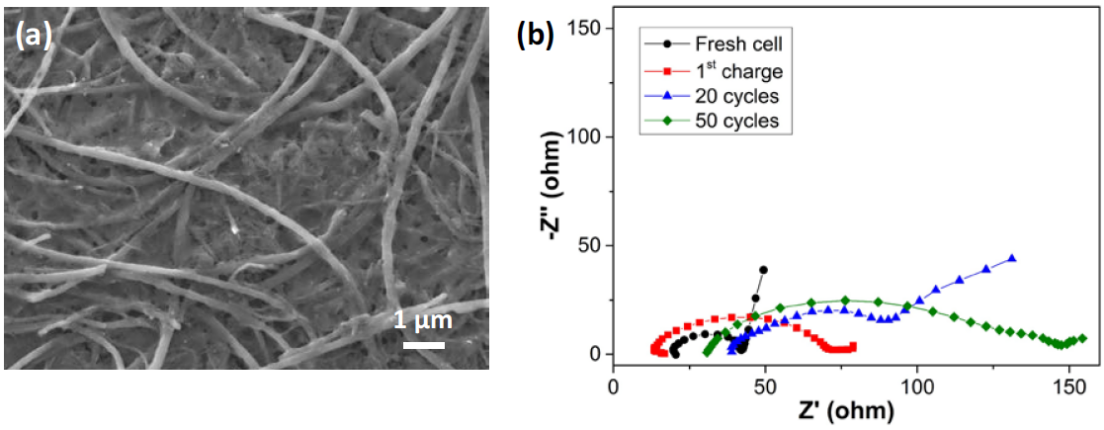

Figure 4.4. (a) SEM image of the SE electrode after one cycle. (b) Nyquist plots of the cell after different cycles.

Fig. 4.4a shows the SEM image of a cycled electrode. After one cycle at the charged state, the electrode was washed by pure DME solvent for 1 hour to remove all soluble species and then scanned under SEM for comparison with the as-prepared electrode shown in Fig. 4.2a. The carbon paper is uniformly filled and covered with insoluble charged products, probably elemental sulfur. The sulfur morphology changed completely from nanoparticle to continuous film. The carbon paper provides a robust matrix holding all cycled products, therefore maintaining stable cycle life as shown in Fig. 4.3. Fig. 4.4b shows the Nyquist plot of the cell after different cycling status. The intercepts of Nyquist plots in the high-frequency are attributed to the bulk resistance of the liquid electrolyte and the semicircles in the high-medium frequency regions are charge transfer resistance of the electrode/electrolyte interfaces [45]. The linear segment in the low-frequency region corresponds to the diffusion limitation within the electrodes. It is shown the cell has a low bulk resistance (20 ohms) and a low charge transfer resistance (22 ohms) before cycling. The monoclinic sulfur nanoparticles in the electrode have a good contact with carbon and the electrolyte, which helps to maintain a low charge transfer resistance. After the 1^{st} cycle at the charged state, the charge transfer resistance increases to 57 ohms which is due to the change in sulfur morphology as shown in Fig. 4.4a. After the 20^{th} and 50^{th} cycle,

the bulk resistance slightly increases to 38 ohms and 31 ohms, respectively, and the charge transfer resistance increases to 82 ohms and 118 ohms, respectively. The bulk resistance increase is due to the depletion of electrolyte and dissolved polysulfide in it, and the charge transfer resistance increases is due to the insulating property at the electrode/electrolyte interface making the charge transfer more difficult.

4.4 Conclusions

In summary, we have successfully prepared binder-free sulfur/carbon composite electrodes by a sulfur sublimation method in air. The sulfur deposited in the electrode mainly has a monoclinic crystal structure and it is in the form of nanoparticles filling all large pores in the carbon paper. Several composite electrodes with a variety of sulfur loading were prepared and evaluated in batteries. The electrodes show high utilization of sulfur, good cycling stability, and rate capability when the sulfur loading is <2.0 mg. The cell with sulfur loading of 1.1 mg cm^{-2} was cycled over 300 cycles at C/2 rate, remaining a reversible capacity of over 700 mAh g^{-1} and a Coulombic efficiency of over 90%. This study demonstrates that the sulfur sublimation method is a clean, scalable, and viable route for making high performance binder-free sulfur/carbon composite electrodes for Li-S batteries.

5. SUMMARY

In this thesis three aspects of Li-S batteries have been studied, including study on polysulfide transport through separators, improved cycling performance by functional polymer, and binder-free sulfur/carbon composite electrode prepared by a sulfur sublimation method.

Firstly, polysulfide transport through separators has been studied. A new method has been developed to evaluate it by measuring the anodic current density produced by the oxidation of polysulfide under an electric field and this oxidation process is diffusion controlled. In the DME/DOL electrolyte, the diffusion coefficient of polysulfide is measured as $3.5 * 10^{-7} cm^2 \ \ s^{-1}$. In a concentration range ($\leq$0.5 M) of the polysulfide solution, the charge of oxidation of polysulfide shows linear relationship with polysulfide concentration. This method can be used as quantitative analysis to evaluate the polysulfide crossover, which is correlated with the porosity, the pore size of separators and battery cycling performance.

Secondly, PVP was used to modify CP current collectors in Li/polysulfide cells. The soluble PVP shows strong affinity with polysulfide in the electrolyte and can form complex. This PVP-modified CP has the ability to improve utilization of sulfur and Coulombic efficiency, to enhance cycling performance and to maintain integrity of the electrode. This study demonstrates that functional polymers, such as PVP et al., can improve cycling stability in Li/polysulfide cells by optimizing the property of CP current collectors.

Finally, a binder-free sulfur/carbon composite electrode was successfully prepared by a sulfur sublimation method. The deposited sulfur mainly shows a monoclinic crystal structure and fills all large pores of carbon paper as nanoparticles. This binder-free electrode shows high utilization of sulfur, good cycling performance and rate capability when its sulfur loading is below 2 mg cm^{-2}. This sulfur sublimation method is

also a clean and scalable way to make high performance binder-free sulfur/composite electrodes for Li-S batteries. Generally speaking, polysulfide transport through separators, functional polymer PVP for improving cycle life and binder-free sulfur/carbon composite electrodes in Li-S batteries have been studied and understood.

LIST OF REFERENCES

LIST OF REFERENCES

[1] F. Liu, B. Yi, D. Xing, J. Yu, Z. Hou, and Y. Fu, "Development of novel self-humidifying composite membranes for fuel cells," *Journal of Power Sources*, vol. 124, no. 1, pp. 81–89, 2003.

[2] J. Yu, B. Yi, D. Xing, F. Liu, Z. Shao, Y. Fu, and H. Zhang, "Degradation mechanism of polystyrene sulfonic acid membrane and application of its composite membranes in fuel cells," *Physical Chemistry Chemical Physics*, vol. 5, no. 3, pp. 611–615, 2003.

[3] Y. Fu, A. Manthiram, and M. D. Guiver, "Blend membranes based on sulfonated poly (ether ether ketone) and polysulfone bearing benzimidazole side groups for proton exchange membrane fuel cells," *Electrochemistry Communications*, vol. 8, no. 8, pp. 1386–1390, 2006.

[4] Y.-Z. Fu, A. Manthiram, and M. D. Guiver, "Acid–base blend membranes based on 2-amino-benzimidazole and sulfonated poly (ether ether ketone) for direct methanol fuel cells," *Electrochemistry Communications*, vol. 9, no. 5, pp. 905–910, 2007.

[5] M. Wu, J. Wang, Z. Wu, H. L. Xin, and D. Wang, "Synergistic enhancement of nitrogen and sulfur co-doped graphene with carbon nanosphere insertion for the electrocatalytic oxygen reduction reaction," *Journal of Materials Chemistry A*, vol. 3, no. 15, pp. 7727–7731, 2015.

[6] Y.-Z. Fu and A. Manthiram, "Nafion–imidazole–H_3PO_4 composite membranes for proton exchange membrane fuel cells," *Journal of The Electrochemical Society*, vol. 154, no. 1, pp. B8–B12, 2007.

[7] Y. Liu, Q. Liu, Z. Li, Y. Ren, J. Xie, H. He, and F. Xu, "Failure study of commercial $LiFePO_4$ cells in over-discharge conditions using electrochemical impedance spectroscopy," *Journal of The Electrochemical Society*, vol. 161, no. 4, pp. A620–A632, 2014.

[8] F. Wu, Y. Liu, R. Chen, S. Chen, and G. Wang, "Preparation and performance of novel Li–Ti–Si–P–O–N thin-film electrolyte for thin-film lithium batteries," *Journal of Power Sources*, vol. 189, no. 1, pp. 467–470, 2009.

[9] Z. Zheng, H. Fang, F. Yang, Z.-K. Liu, and Y. Wang, "Amorphous $LiLaTiO_3$ as solid electrolyte material," *Journal of The Electrochemical Society*, vol. 161, no. 4, pp. A473–A479, 2014.

[10] B. Yan, C. Lim, L. Yin, and L. Zhu, "Simulation of heat generation in a reconstructed $LiCoO_2$ cathode during galvanostatic discharge," *Electrochimica Acta*, vol. 100, pp. 171–179, 2013.

[11] B. Yan, C. Lim, Z. Song, and L. Zhu, "Analysis of polarization in realistic li ion battery electrode microstructure using numerical simulation," *Electrochimica Acta*, vol. 185, pp. 125–141, 2015.

[12] H. He, Y. Liu, Q. Liu, Z. Li, F. Xu, C. Dun, Y. Ren, M.-X. Wang, and J. Xie, "Failure investigation of $LiFePO_4$ cells in over-discharge conditions," *Journal of The Electrochemical Society*, vol. 160, no. 6, pp. A793–A804, 2013.

[13] Y. Fu, C. Zu, and A. Manthiram, "In situ-formed Li_2S in lithiated graphite electrodes for lithium–sulfur batteries," *Journal of the American Chemical Society*, vol. 135, no. 48, pp. 18 044–18 047, 2013.

[14] Y. Fu, Y.-S. Su, and A. Manthiram, "Li_2S-carbon sandwiched electrodes with superior performance for lithium-sulfur batteries," *Advanced Energy Materials*, vol. 4, no. 1, 2014.

[15] A. Bhargav, W. Guo, and Y. Fu, "Chemically synthesized lithium peroxide composite cathodes for closed system Li–O_2 batteries," *Chemical Communications*, 2016.

[16] C. Jia, Q. Liu, C.-J. Sun, F. Yang, Y. Ren, S. M. Heald, Y. Liu, Z.-F. Li, W. Lu, and J. Xie, "In situ x-ray near-edge absorption spectroscopy investigation of the state of charge of all-vanadium redox flow batteries," *ACS Applied Materials & Interfaces*, vol. 6, no. 20, pp. 17 920–17 925, 2014.

[17] A. Manthiram, "Materials challenges and opportunities of lithium ion batteries," *The Journal of Physical Chemistry Letters*, vol. 2, no. 3, pp. 176–184, 2011.

[18] A. Manthiram, Y. Fu, S.-H. Chung, C. Zu, and Y.-S. Su, "Rechargeable lithium–sulfur batteries," *Chemical Reviews*, vol. 114, no. 23, pp. 11 751–11 787, 2014.

[19] X. Ji and L. F. Nazar, "Advances in Li–S batteries," *Journal of Materials Chemistry*, vol. 20, no. 44, pp. 9821–9826, 2010.

[20] J. B. Goodenough and Y. Kim, "Challenges for rechargeable Li batteries," *Chemistry of Materials*, vol. 22, no. 3, pp. 587–603, 2009.

[21] H. Li, Z. Wang, L. Chen, and X. Huang, "Research on advanced materials for Li-ion batteries," *Advanced Materials*, vol. 21, no. 45, pp. 4593–4607, 2009.

[22] P. G. Bruce, S. A. Freunberger, L. J. Hardwick, and J.-M. Tarascon, "Li-O_2 and Li-S batteries with high energy storage," *Nature Materials*, vol. 11, no. 1, pp. 19–29, 2012.

[23] A. Manthiram, Y. Fu, and Y.-S. Su, "Challenges and prospects of lithium–sulfur batteries," *Accounts of Chemical Research*, vol. 46, no. 5, pp. 1125–1134, 2012.

[24] R. Rauh, K. Abraham, G. Pearson, J. Surprenant, and S. Brummer, "A lithium/dissolved sulfur battery with an organic electrolyte," *Journal of the Electrochemical Society*, vol. 126, no. 4, pp. 523–527, 1979.

[25] Y. V. Mikhaylik and J. R. Akridge, "Polysulfide shuttle study in the Li/S battery system," *Journal of the Electrochemical Society*, vol. 151, no. 11, pp. A1969–A1976, 2004.

[26] Y.-S. Su, Y. Fu, B. Guo, S. Dai, and A. Manthiram, "Fast, reversible lithium storage with a sulfur/long-chain-polysulfide redox couple," *Chemistry–A European Journal*, vol. 19, no. 26, pp. 8621–8626, 2013.

[27] Y. Cui and Y. Fu, "Enhanced cyclability of Li/polysulfide batteries by a polymer-modified carbon paper current collector," *ACS Applied Materials & Interfaces*, vol. 7, no. 36, pp. 20 369–20 376, 2015.

[28] N. Jayaprakash, J. Shen, S. S. Moganty, A. Corona, and L. A. Archer, "Porous hollow carbon@ sulfur composites for high-power lithium–sulfur batteries," *Angewandte Chemie International Edition*, vol. 50, no. 26, pp. 5904–5908, 2011.

[29] S. Xin, L. Gu, N.-H. Zhao, Y.-X. Yin, L.-J. Zhou, Y.-G. Guo, and L.-J. Wan, "Smaller sulfur molecules promise better lithium–sulfur batteries," *Journal of the American Chemical Society*, vol. 134, no. 45, pp. 18 510–18 513, 2012.

[30] Y.-S. Su and A. Manthiram, "Lithium–sulphur batteries with a microporous carbon paper as a bifunctional interlayer," *Nature Communications*, vol. 3, p. 1166, 2012.

[31] Z. Jin, K. Xie, and X. Hong, "Electrochemical performance of lithium/sulfur batteries using perfluorinated ionomer electrolyte with lithium sulfonyl dicyanomethide functional groups as functional separator," *RSC Advances*, vol. 3, no. 23, pp. 8889–8898, 2013.

[32] X. Ren, T. E. Springer, T. A. Zawodzinski, and S. Gottesfeld, "Methanol transport through nation membranes. electro-osmotic drag effects on potential step measurements," *Journal of the Electrochemical Society*, vol. 147, no. 2, pp. 466–474, 2000.

[33] Y.-Z. Fu and A. Manthiram, "Synthesis and characterization of sulfonated polysulfone membranes for direct methanol fuel cells," *Journal of Power Sources*, vol. 157, no. 1, pp. 222–225, 2006.

[34] Y.-Z. Fu, A. Manthiram, and M. Guiver, "Blend membranes based on sulfonated poly (ether ether ketone) and polysulfone bearing benzimidazole side groups for dmfcs," *Electrochemical and Solid-State Letters*, vol. 10, no. 4, pp. B70–B73, 2007.

[35] Y. Fu, Y.-S. Su, and A. Manthiram, "Highly reversible lithium/dissolved polysulfide batteries with carbon nanotube electrodes," *Angewandte Chemie International Edition*, vol. 52, no. 27, pp. 6930–6935, 2013.

[36] D. Moy, A. Manivannan, and S. Narayanan, "Direct measurement of polysulfide shuttle current: A window into understanding the performance of lithium-sulfur cells," *Journal of The Electrochemical Society*, vol. 162, no. 1, pp. A1–A7, 2015.

[37] R. Dominko, R. Demir-Cakan, M. Morcrette, and J.-M. Tarascon, "Analytical detection of soluble polysulphides in a modified swagelok cell," *Electrochemistry Communications*, vol. 13, no. 2, pp. 117–120, 2011.

[38] L. Xiao, Y. Cao, J. Xiao, B. Schwenzer, M. H. Engelhard, L. V. Saraf, Z. Nie, G. J. Exarhos, and J. Liu, "A soft approach to encapsulate sulfur: polyaniline nanotubes for lithium-sulfur batteries with long cycle life," *Advanced Materials*, vol. 24, no. 9, pp. 1176–1181, 2012.

[39] J. Guo, Z. Yang, Y. Yu, H. D. Abruna, and L. A. Archer, "Lithium–sulfur battery cathode enabled by lithium–nitrile interaction," *Journal of the American Chemical Society*, vol. 135, no. 2, pp. 763–767, 2012.

[40] X. Cui, Z. Shan, L. Cui, and J. Tian, "Enhanced electrochemical performance of sulfur/carbon nanocomposite material prepared via chemical deposition with a vacuum soaking step," *Electrochimica Acta*, vol. 105, pp. 23–30, 2013.

[41] W. Zhou, Y. Yu, H. Chen, F. J. DiSalvo, and H. D. Abruna, "Yolk–shell structure of polyaniline-coated sulfur for lithium–sulfur batteries," *Journal of the American Chemical Society*, vol. 135, no. 44, pp. 16 736–16 743, 2013.

[42] S.-H. Chung and A. Manthiram, "A hierarchical carbonized paper with controllable thickness as a modulable interlayer system for high performance Li–S batteries," *Chemical Communications*, vol. 50, no. 32, pp. 4184–4187, 2014.

[43] C. Huang, J. Xiao, Y. Shao, J. Zheng, W. D. Bennett, D. Lu, L. V. Saraf, M. Engelhard, L. Ji, J. Zhang *et al.*, "Manipulating surface reactions in lithium–sulphur batteries using hybrid anode structures," *Nature Communications*, vol. 5, 2014.

[44] X. Wang, Z. Wang, and L. Chen, "Reduced graphene oxide film as a shuttle-inhibiting interlayer in a lithium–sulfur battery," *Journal of Power Sources*, vol. 242, pp. 65–69, 2013.

[45] Y. Fu and A. Manthiram, "Enhanced cyclability of lithium–sulfur batteries by a polymer acid-doped polypyrrole mixed ionic–electronic conductor," *Chemistry of Materials*, vol. 24, no. 15, pp. 3081–3087, 2012.

[46] X. Liang, Y. Liu, Z. Wen, L. Huang, X. Wang, and H. Zhang, "A nano-structured and highly ordered polypyrrole-sulfur cathode for lithium–sulfur batteries," *Journal of Power Sources*, vol. 196, no. 16, pp. 6951–6955, 2011.

[47] Y. Fu, Y.-S. Su, and A. Manthiram, "Sulfur–carbon nanocomposite cathodes improved by an amphiphilic block copolymer for high-rate lithium–sulfur batteries," *ACS Applied Materials & Interfaces*, vol. 4, no. 11, pp. 6046–6052, 2012.

[48] F. Wu, J. Chen, R. Chen, S. Wu, L. Li, S. Chen, and T. Zhao, "Sulfur/polythiophene with a core/shell structure: synthesis and electrochemical properties of the cathode for rechargeable lithium batteries," *The Journal of Physical Chemistry C*, vol. 115, no. 13, pp. 6057–6063, 2011.

[49] Y. Fu and A. Manthiram, "Core-shell structured sulfur-polypyrrole composite cathodes for lithium-sulfur batteries," *Rsc Advances*, vol. 2, no. 14, pp. 5927–5929, 2012.

[50] W. Li, Q. Zhang, G. Zheng, Z. W. Seh, H. Yao, and Y. Cui, "Understanding the role of different conductive polymers in improving the nanostructured sulfur cathode performance," *Nano Letters*, vol. 13, no. 11, pp. 5534–5540, 2013.

[51] Y. Fu and A. Manthiram, "Orthorhombic bipyramidal sulfur coated with polypyrrole nanolayers as a cathode material for lithium–sulfur batteries," *The Journal of Physical Chemistry C*, vol. 116, no. 16, pp. 8910–8915, 2012.

[52] D. Bresser, S. Passerini, and B. Scrosati, "Recent progress and remaining challenges in sulfur-based lithium secondary batteries–a review," *Chemical Communications*, vol. 49, no. 90, pp. 10 545–10 562, 2013.

[53] S.-E. Cheon, J.-H. Cho, K.-S. Ko, C.-W. Kwon, D.-R. Chang, H.-T. Kim, and S.-W. Kim, "Structural factors of sulfur cathodes with poly (ethylene oxide) binder for performance of rechargeable lithium sulfur batteries," *Journal of the Electrochemical Society*, vol. 149, no. 11, pp. A1437–A1441, 2002.

[54] Z. W. Seh, Q. Zhang, W. Li, G. Zheng, H. Yao, and Y. Cui, "Stable cycling of lithium sulfide cathodes through strong affinity with a bifunctional binder," *Chemical Science*, vol. 4, no. 9, pp. 3673–3677, 2013.

[55] Y. Cui and Y. Fu, "Polysulfide transport through separators measured by a linear voltage sweep method," *Journal of Power Sources*, vol. 286, pp. 557–560, 2015.

[56] S. S. Zhang, "Role of $LiNO_3$ in rechargeable lithium/sulfur battery," *Electrochimica Acta*, vol. 70, pp. 344–348, 2012.

[57] Y.-X. Yin, S. Xin, Y.-G. Guo, and L.-J. Wan, "Lithium–sulfur batteries: Electrochemistry, materials, and prospects," *Angewandte Chemie International Edition*, vol. 52, no. 50, pp. 13 186–13 200, 2013.

[58] X. Ji, K. T. Lee, and L. F. Nazar, "A highly ordered nanostructured carbon–sulphur cathode for lithium–sulphur batteries," *Nature Materials*, vol. 8, no. 6, pp. 500–506, 2009.

[59] C. Liang, N. J. Dudney, and J. Y. Howe, "Hierarchically structured sulfur/carbon nanocomposite material for high-energy lithium battery," *Chemistry of Materials*, vol. 21, no. 19, pp. 4724–4730, 2009.

[60] H. Wang, Y. Yang, Y. Liang, J. T. Robinson, Y. Li, A. Jackson, Y. Cui, and H. Dai, "Graphene-wrapped sulfur particles as a rechargeable lithium–sulfur battery cathode material with high capacity and cycling stability," *Nano Letters*, vol. 11, no. 7, pp. 2644–2647, 2011.

[61] G. Zhou, L. Li, D.-W. Wang, X.-y. Shan, S. Pei, F. Li, and H.-M. Cheng, "A flexible sulfur-graphene-polypropylene separator integrated electrode for advanced Li–S batteries," *Advanced Materials*, vol. 27, no. 4, pp. 641–647, 2015.

[62] M. Wu, Y. Cui, and Y. Fu, "Li2s nanocrystals confined in free-standing carbon paper for high performance lithium–sulfur batteries," *ACS Applied Materials & Interfaces*, vol. 7, no. 38, pp. 21 479–21 486, 2015.

[63] D.-W. Wang, Q. Zeng, G. Zhou, L. Yin, F. Li, H.-M. Cheng, I. R. Gentle, and G. Q. M. Lu, "Carbon–sulfur composites for li–s batteries: status and prospects," *Journal of Materials Chemistry A*, vol. 1, no. 33, pp. 9382–9394, 2013.

[64] M. Hagen, S. Dörfler, H. Althues, J. Tübke, M. Hoffmann, S. Kaskel, and K. Pinkwart, "Lithium–sulphur batteries–binder free carbon nanotubes electrode examined with various electrolytes," *Journal of Power Sources*, vol. 213, pp. 239–248, 2012.

[65] K. Fu, Y. Li, M. Dirican, C. Chen, Y. Lu, J. Zhu, Y. Li, L. Cao, P. D. Bradford, and X. Zhang, "Sulfur gradient-distributed cnf composite: a self-inhibiting cathode for binder-free lithium–sulfur batteries," *Chemical Communications*, vol. 50, no. 71, pp. 10 277–10 280, 2014.

[66] A. Fallah-Shojaei, K. Tabatabaeian, F. Shirini, and S. Z. Hejazi, "Multi-walled carbon nanotube supported Fe_3O_4 NPs: an efficient and reusable catalyst for the one-pot synthesis of 4 H-pyran derivatives," *RSC Advances*, vol. 4, no. 19, pp. 9509–9516, 2014.

[67] S. Moon, Y. H. Jung, W. K. Jung, D. S. Jung, J. W. Choi, and D. K. Kim, "Encapsulated monoclinic sulfur for stable cycling of Li–S rechargeable batteries," *Advanced Materials*, vol. 25, no. 45, pp. 6547–6553, 2013.

[68] S. Zhao, C. Li, W. Wang, H. Zhang, M. Gao, X. Xiong, A. Wang, K. Yuan, Y. Huang, and F. Wang, "A novel porous nanocomposite of sulfur/carbon obtained from fish scales for lithium–sulfur batteries," *Journal of Materials Chemistry A*, vol. 1, no. 10, pp. 3334–3339, 2013.

[69] D.-W. Wang, G. Zhou, F. Li, K.-H. Wu, G. Q. M. Lu, H.-M. Cheng, and I. R. Gentle, "A microporous–mesoporous carbon with graphitic structure for a high-rate stable sulfur cathode in carbonate solvent-based Li–S batteries," *Physical Chemistry Chemical Physics*, vol. 14, no. 24, pp. 8703–8710, 2012.